CHAPWTER 16

Structural Features of Chalcogen Bonds and Weak Interactions Involving Chalcogens

M. CARLA ARAGONI*[a] AND YURY TORUBAEV[b]

[a] Dipartimento di Scienze Chimiche e Geologiche, Cittadella Universitaria Monserrato, SS. 554 – bivio Sestu, 09042 Monserrato, Cagliari, Italy; [b] N.S. Kurnakov Institute of General and Inorganic Chemistry, Russian Academy of Sciences, Leninsky Prospect. 31, 119991, Moscow, Russia
*Email: aragoni@unica.it

16.1 Introduction

Chalcogen (Ch) elements of group 16 of the periodic table typically form neutral organic compounds such as chalcogenone $R_1R_2C{=}Ch$, chalcogenoethers $R_1{-}Ch{-}R_2$, and chalcogen oxides $R_1{-}(Ch{=}O){-}R_2$, with anisotropic distribution of the electron density that determines the presence, on the Ch atom's surface, of areas of higher and lower electron density where the electrostatic potential can be negative and positive, respectively.[1] Regions of positive, or less negative, electrostatic potential, commonly named σ-holes, are frequently disposed opposite to these $R_1{-}Ch$ bonds and can attractively interact with electron-rich sites such as Nu atoms and anions possessing a lone pair (Lp) of electrons, in the formation of the so-called chalcogen bonds (ChB, Scheme 16.1).

These attractive interactions involving chalcogen atoms as electrophiles can be identified by considering the close contacts between group 16 elements and Lp-possessing atoms in crystalline solids. The earliest

Chalcogen Chemistry: Fundamentals and Applications
Edited by Vito Lippolis, Claudio Santi, Eder J. Lenardão and Antonio L. Braga

Published by the Royal Society of Chemistry, www.rsc.org

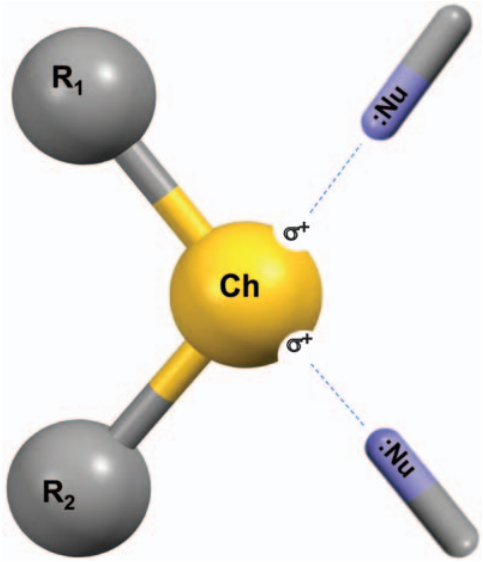

Scheme 16.1 Schematic representation of ChB formation.

crystallographic contribution to the understanding of these kinds of interactions involving chalcogen atoms was reported in 1977,[2] and describes the electrophilic attack to divalent sulfur in R_1–S–R_2 moieties roughly perpendicular to the R_1–S–R_2 plane and the nucleophilic attack along the extension of the S–R_1 or S–R_2 covalent bonds. However, attention to interactions driven by electrophilic chalcogen atoms started to increase only after 2007, when a model of the electronic basis of ChB was proposed.[3] Nowadays, ChBs are considered highly-directional noncovalent interactions between a covalently bonded Ch atom (O, S, Se, or Te) acting as an electrophilic species and a nucleophilic electron-rich donor centre Nu (Nu = electron donor atom, anion, π-system, radical, *etc.*) along the axes of the covalent bonds (Scheme 16.1) in agreement with the recent definition provided by the IUPAC.[4] Chalcogen-bonded systems typically display interatomic distances that are intermediate between those of typical single bonds and the sum of van der Waals radii.[5] In general, this interaction is strengthened by the presence of an electron-withdrawing group on the electron-acceptor Ch atom and it increases with the atomic number of the Ch species, from O to Te.[6] Following the surge of interest in halogen bonding (HaB), research on ChB is undergoing very fast expansion. Several recent reviews have covered fundamental aspects and applications of this type of interaction and highlighted examples from the literature.[7–9]

In this chapter the structural features of ChB will be mainly discussed highlighting the differences depending on the chalcogen element.

16.2 A Structural Approach to Chalcogen Bonds

ChB interactions involve electrostatic, covalent, and dispersion contributions (see Chapter 17 of this book). The electrostatic contribution comes from a Coulomb attraction between the negative electrostatic potential of the

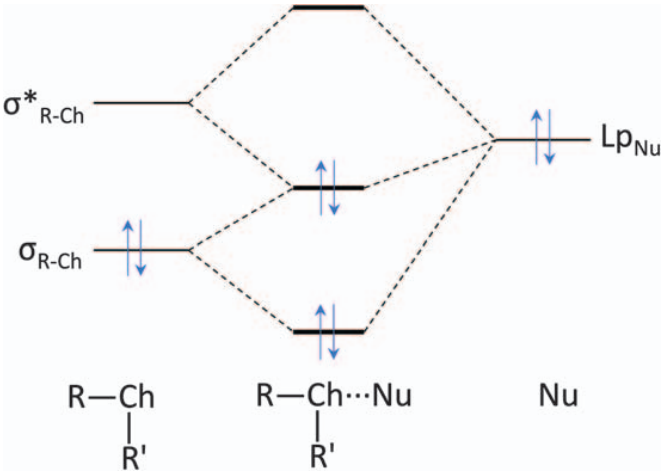

Figure 16.1 Perturbation molecular orbital scheme showing the 2e-delocalization of an electron lone pair of the nucleophile (Lp_{Nu}) into the σ^*_{R-Ch} orbital of the chalcogen.

Lewis base that behaves as the nucleophile (Nu), located at the lone pairs Lp_{Nu} or π-bond of Nu, and the positive electrostatic potential at the σ-hole region collinear to the covalent bond formed between the Ch atom and its most electronegative substituent.[10,11] The covalent contribution derives from the charge-transfer (CT) from the Lp_{Nu} of electrons localized on an occupied molecular orbital (MO) of the donor to the σ*(R–Ch) unoccupied MO (Figure 16.1) leading to a partial electron delocalization proportional to the Lp_{Nu}_σ* orbital overlap, which in turn is inversely proportional to the energy gap between the Lp_{Nu} and the σ*(R–Ch) orbitals.

The dominant contributions to ChB are strongly dependent on the nature of the R–Ch···Nu system and the ChB becomes stronger with increasing polarizability of the chalcogen atom (Te > Se > S) and polarizing effect of the R substituent, and higher donor ability of Lp_{Nu}.

This observation recalls the analogous finding for halogen bonding in crystalline halides RHa, where Ha = Cl, Br, or I. In these systems, close intermolecular contacts with nucleophiles tend to be along the extensions of the R–Ha bonds. These interactions known as halogen bonding HaB typically involves Ha and a Lewis base, and an increase in likelihood and in strength in the order Ha = Cl < Br < I.[12]

Information on the covalent or electrostatic nature of the ChBs can be obtained from the theoretical analysis of the energy density distribution at the electron density critical bond point according to the Quantum Theory of Atoms in Molecule (QTAIM).[11,13]

As previously recalled, compounds containing ChB show a marked directionality, the ChB being oriented approximately along the extensions of the R_1–Ch or R_2–Ch bonds (usually within a ±20° range). A "close" contact occurs when the internuclear distance is shorter than the sum of the van der Waals (vdW) radii of the relevant atomic species and implies a noncovalent interaction.

In the following, a systematic, although necessary concise, overview is presented about the structural features of the linear fragments R–Ch···Nu

(Ch = S, Se, Te; R–Ch···Nu in the range 160–180°) found in the Cambridge Structural Database (CSD) were a chalcogen bond is present. For each chalcogen, the analyses of the most frequently encountered fragments are presented sorted as a function of the nature of the atom directly bound. In order to better evaluate the strength of the ChBs involved and to compare the structural data of fragments R–Ch···Nu involving different atoms, the results were standardized for the relevant covalent and van der Waals radii (r_{cov} and r_{vdW}, respectively) by introducing the functions δ_{R-Ch} and $\delta_{Ch\cdots Nu}$ calculated by normalizing the differences between the involved R–Ch (Ch···Nu) distances d_{R-Ch} ($d_{Ch\cdots Nu}$) and the sum of the relevant covalent (vdW) radii (eqn (16.1) and (16.2)):[14]

$$\delta_{R-Ch} = \frac{d_{R-Ch} - (r_{cov}R + r_{cov}Ch)}{r_{cov}R + r_{cov}Ch} \times 100 \qquad (16.1)$$

$$\delta_{Ch\cdots Nu} = \frac{d_{Ch\cdots Nu} - (r_{vdW}Ch + r_{vdW}Nu)}{r_{vdW}Ch + r_{vdW}Nu} \times 100 \qquad (16.2)$$

The values of δ_{R-Ch} and $\delta_{Ch\cdots Nu}$, defined above, represent the relative variations of R–Ch and Ch···Nu distances independently on the atomic species involved in the bonds and interactions, thus allowing for a direct comparison between strictly related systems.

Specific single/double bond covalent radii for the atoms engaged in R–Ch bonds were used depending on the nature of the bond in the considered fragments.[5]

A list of typical ChB donors and acceptors,[4] shows that R–Ch molecular entities commonly involved in ChB are chalcogen-containing heterocycles and azoles, and their fused polycyclic derivatives; chalcogen-anhydrides, and their analogues with sulfonyl groups in place of carbonyl ones; chalcogen-cyanates and chalcogen oxides, where the R atom is directly bonded to the chalcogen is mainly either a carbon, a nitrogen, or another chalcogen atom. Entities behaving as ChB acceptors are nucleophiles with Lp-possessing atoms and anions where the atom Nu directly involved in ChB is essentially either a pnictogen (usually nitrogen), another chalcogen, or a halogen atom. Unsaturated systems where the acceptor is a multiple bond or an aromatic entity will not be examined here, and the reader is directed to specific publications to get a side view of this subject.[15–18] In the following sections a systematic survey of the structural features of the chalcogen bonds in the linear systems R–Ch···Nu (R = C, N, O, S, Se, Te and Nu = N, O, S, Se, Te, F, Cl, Br, I) is reported, categorized on the nature of the involved chalcogen atom (Ch = S, Se, Te). Among the about 34 000 fragments found, more than 80% are compounds where the Ch atom involved in the ChB is sulfur.

16.2.1 R–S···Nu fragments

The results of the search on the CSD,[19] for linear fragments R–S···Nu with R = B, C, N, P, As, O, S, Se, Te and Nu = N, P, As, Sb, O, S, Se, Te, F, Cl, Br,

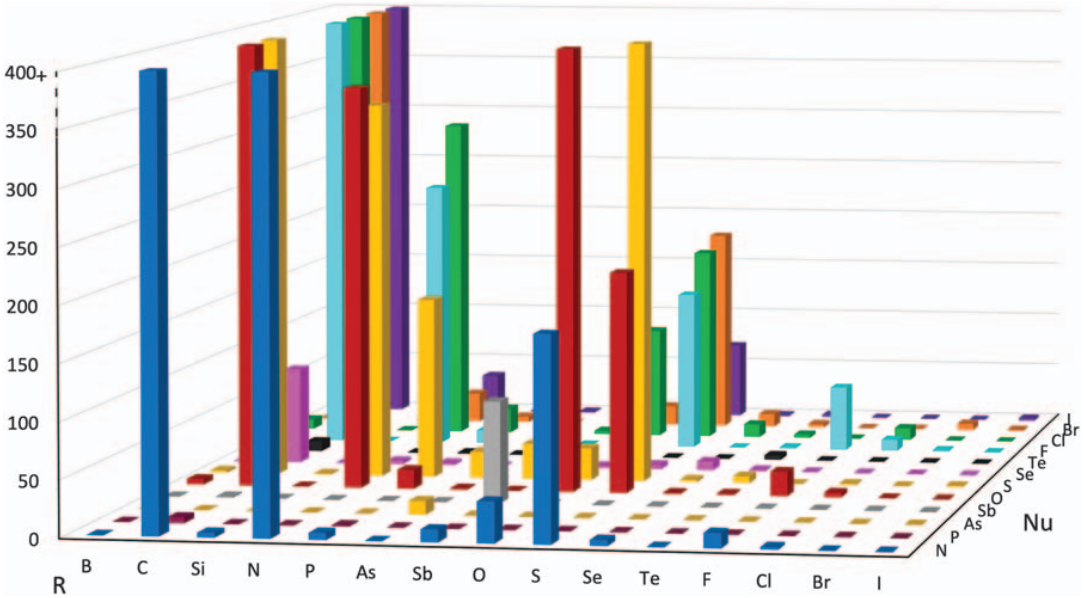

Figure 16.2 Linear R–S···Nu fragment occurrence (R = B, C, N, P, As, Sb, O, S, Se, Te, F, Cl, Br, I; Nu = N, P, As, Sb, O, S, Se, Te, F, Cl, Br, I) deposited at the CSD.

I are shown in Figure 16.2, where the numeric prevalence of R–S···Nu systems with R = C, N, O, and S is evidenced. Among the almost thirty thousand fragments (27 763 entries) found in the database, about 80% (21 993 items) belong to C–S···Nu systems with a carbon atom directly bound to the sulfur atom. The remaining 20% is mainly constituted of N–S···Nu (9%) and Ch–S···Nu (10%) fragments with a very minor contribute coming from all the other systems (1%).

Therefore, the survey here presented will be limited to the most frequently encountered systems belonging to the fragments RS···Nu, with R = C, N, O, and S and Nu = N, Ch, and Ha.

16.2.1.1 C–S···Nu

A total of 21 993 C–S···Nu linear fragments showing structural features fitting the criteria described above and pointing to the presence of ChB interactions can be found to date in the CSD.[19] About 70% of these fragments involve ChB acceptors with Nu = chalcogen as the donor atoms. Following in abundance are C–S···Ha fragments (Ha = halogen, 21%), followed by C–S···Pn (Pn = pnictogen, 9%) fragments, with a net prevalence of nitrogen as the nucleophile donor atom. The compounds included in this survey are various and belong to the categories of sulfur-containing heterocycles such as thiophene and thiazole, and tetrathiafulvalene derivatives, thio- and dithio-carbamates, thioureas, dialkyl sulfoxides, thiocyanates, thioethers, and sulfur-containing macrocycles.

The CSD lists 15 417 linear fragments C–S···Ch, with a net prevalence for ChB acceptors featuring Ch = S (C–S···S 57%) and O (C–S···O 42%). Fragments involving halogen acceptors C–S···Ha are lesser, but still abundant with 4595 items (C–S···F 32.9%, C–S···Cl 40.7%, C–S···Br 14.4%, and

C–S···I 12.0%). Less numerous are the fragments involving pnictogen acceptors C–S···Pn, with 1981 items almost entirely concerning nitrogen (C–S···N 99.7%, C–S···P 0.25%, and C–S···Sb 0.05%). The mean distances calculated within the fragments C–S···Nu in the sub-categories are quite similar to each other, with values $d_{C–S} = 1.734$ (0.03), 1.746 (0.03), and 1.747 (0.05) Å, and $d_{S\cdots Nu} = 3.20$ (0.12), 3.33 (0.19), and 3.36 (0.22) Å for Nu = Pn, Ch, and Ha, respectively, (standard deviations s in parentheses). This notwithstanding, the scatterplots of $d_{S\cdots Nu}$ *vs.* $d_{C–S}$ for Nu = Pn (a), Ch (b), and Ha (c) show different ranges of existence depending on the nature of the interacting Nu atoms (evidenced by using different colours in Figure 16.3).

The mean values calculated for the C–S and S···Nu distances in the fragments C–S···Nu are summarized in Table 16.1, along with the mean of the delta $\delta_{C–S}$ and $\delta_{S\cdots Nu}$ values calculated, as explained above (eqn (16.1)

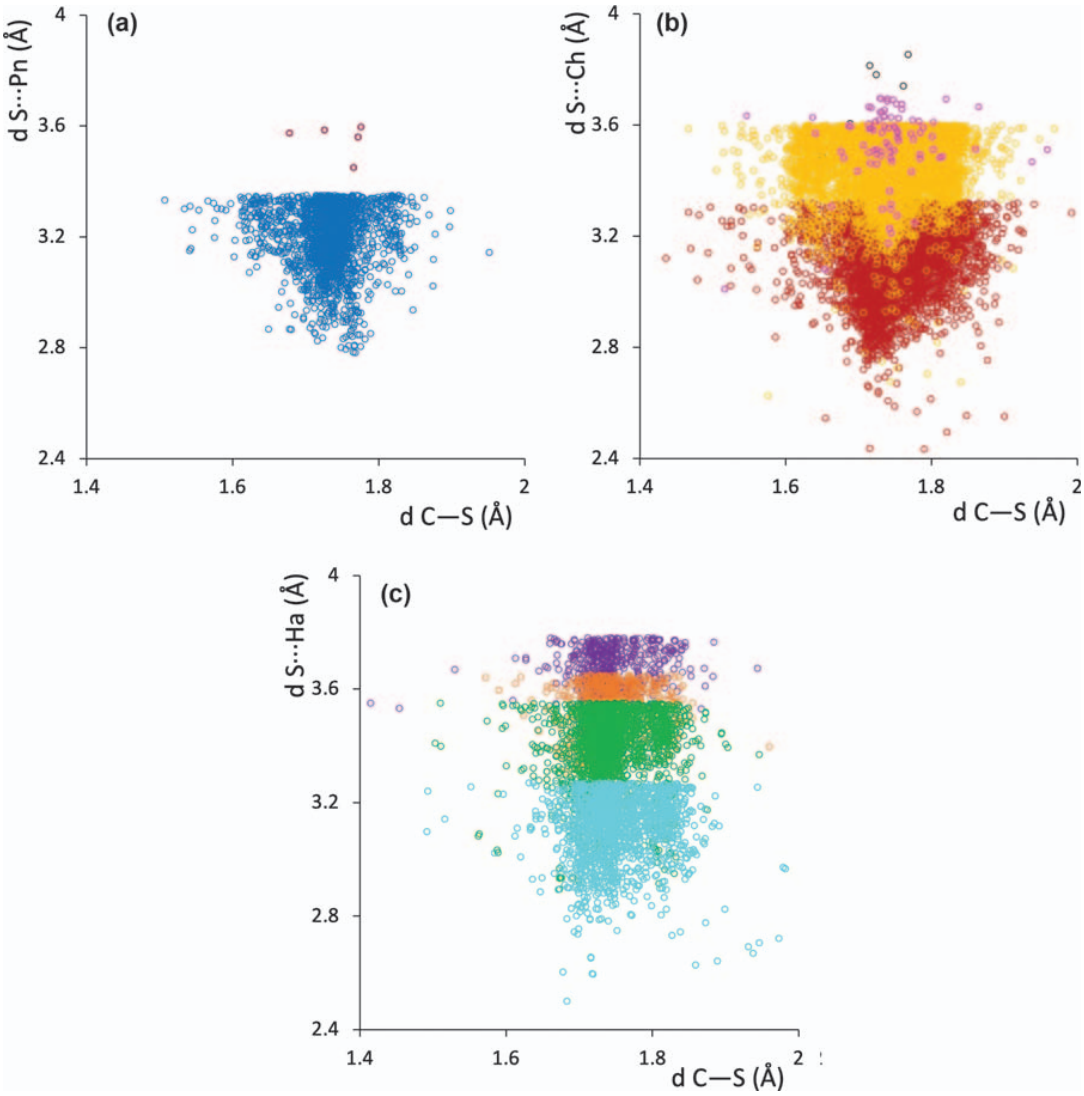

Figure 16.3 Scatterplots of $d_{S\cdots Nu}$ *vs.* $d_{C–S}$ distances in the C–S···Nu fragments for Nu = Pn (a); Ch (b); Ha (c). Nu colour codes: N = blue, P = purple in (a); O = red, S = yellow, Se = magenta, Te = black in (b); F = cyan, Cl = green, Br = orange, I = violet in (c).

Table 16.1 Occurrence, mean distances d [Å] (standard deviation, s), and δ values for C–S···Nu fragments.

Nu	Occurrence	d_{C-S} (s)	$d_{S\cdots Nu}$ (s)	δ_{C-S} (%)	$\delta_{S\cdots Nu}$ (%)
O	6537	1.751 (0.05)	3.149 (0.10)	5.07	− 5.15
S	8784	1.742 (0.05)	3.461 (0.11)	5.49	− 3.87
Se	87	1.743 (0.06)	3.526 (0.10)	5.85	− 4.69
Te	9	1.709 (0.05)	3.639 (0.16)	3.29	− 5.71
N	1975	1.734 (0.05)	3.197 (0.11)	6.13	− 4.57
P	5	1.744 (0.04)	3.552 (0.06)	5.17	− 1.32
F	1511	1.753 (0.053)	3.112 (0.12)	5.22	− 4.83
Cl	1871	1.746 (0.047)	3.402 (0.12)	5.50	− 4.18
Br	661	1.743 (0.04)	3.519 (0.10)	5.58	− 3.58
I	552	1.741 (0.054)	3.662 (0.08)	5.70	− 3.13

and (16.2)), in order to compare systems involving atoms of different radii. Figure 16.4 shows the scatterplots of δ_{C-S} *vs.* $\delta_{S\cdots Nu}$.

The scatterplots clearly show that the relative C–S elongation, expressed as δ_{C-S}, varies in a range between 0% and 9%. Depending on the nature of the molecule containing the sulfur atom involved in the ChB, three main groups are roughly defined in the scatterplots. Thiocyanates, tetrathiafulvalene derivatives, sulfonyl anions and compounds featuring the sulfur atom in planar and/or highly delocalized systems show marked elongations. On the contrary, systems with the sulfur atom bound to poorly electron-withdrawing or even electron-donating substituents show small elongations with some negative values related to systems such as dimethyl sulfoxide (DMSO) where the sulfur atoms are involved in very weak ChBs.

Without taking into account the Nu with limited occurrence, $\delta_{S\cdots Nu}$ values show the dependence of the interaction strength on σ-hole bond acceptors with a $\delta_{S\cdots Nu}$ shortening decreasing in the order O < F < Se < N < Cl < S < Br < I, according to the previously reported study by Wood on σ-hole interactions in small-molecule compounds containing divalent sulfur groups R_1–S–R_2.[20]

16.2.1.2 N–S···Nu

A number of 2845 linear fragments bearing a Pn–S···Nu ChB, with a net prevalence for the systems bearing a N–S covalent bond (2426 items, 85%) can be found in the CSD.[19] The P–S···Nu systems represent only a minority of these data (8%) and will not be dealt with in this chapter; the reader is directed to the recent work of W. T. Pennington.[21] Among the N–S···Nu fragments, 1116 (46%) N–S···N, 707 (29%) N–S···Ch, and 603 (25%) N–S···Ha items can be identified. The compounds comprised in this category are various and mainly belong to the class of sulfanilamide derivatives, or sulfur and nitrogen containing heterocycles such as thiazoles and a fused polycyclic derivative thereof.

The number of linear fragments bearing a N–S···N ChB amounts to 1116, those involving chalcogen acceptors C–S···Ch amounts to 707 (N–S···O 51.3%, N–S···S 48.2%, and N–S···Se 0.5%), and those involving halogen

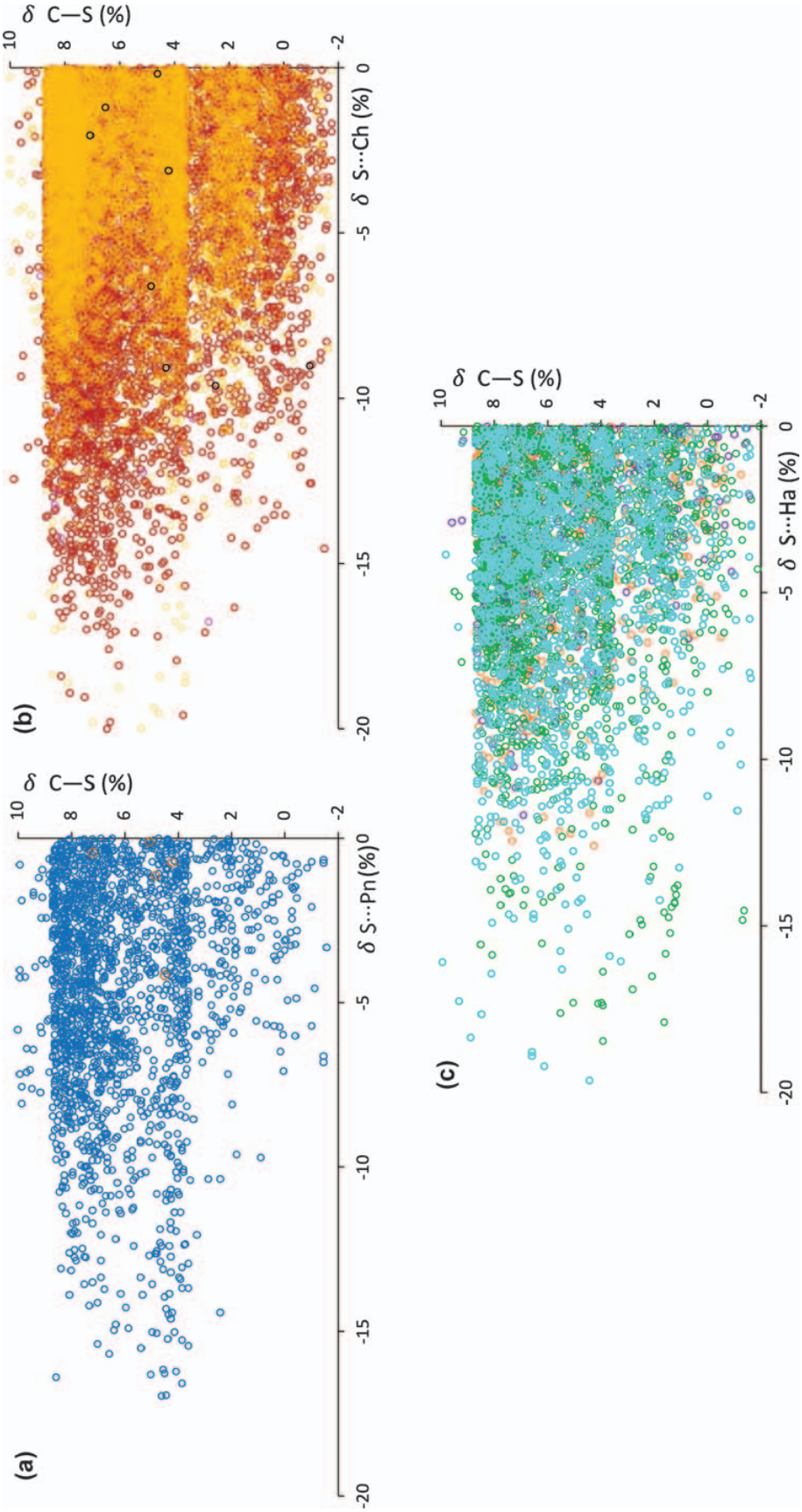

Figure 16.4 Scatterplots of δ_{C-S} *vs.* $\delta_{S\cdots Nu}$ calculated for the C–S···Nu fragments for Nu = Pn (a); Ch (b); Ha (c). Nu colour codes: N = blue, P = purple in (a); O = red, S = yellow, Se = magenta, Te = black in (b); F = cyan, Cl = green, Br = orange, I = violet in (c).

nucleophiles C–S···Ha amounts to 603 (C–S···F 40.7, C–S···F 32.9%, C–S···Br 14.4%, and C–S···I 12.0%). The mean distances $d_{N–S}$ and $d_{S···Nu}$ calculated within the fragments N–S···Nu in the three sub-categories with Nu = N, Ch, and Ha present similar values [$d_{N–S}$ = 1.629 (0.03), 1.641 (0.04), and 1.615 (0.04) Å; $d_{S···Nu}$ = 3.10 (0.13), 3.19 (0.28), and 3.16 (0.26) Å for Nu = N, Ch, and Ha, respectively]. Both covalent N–S and non-covalent S···Nu distances within N–S···Nu moieties are notably shorter than those found in the analogous C–S···Nu fragments, notwithstanding the similar values of the covalent radii of C and N atoms directly bonded to sulfur, the similarity of the involved substrates, and the same van der Waals radii of the interacting species. This experimental evidence confirms the expected ChB interaction increasing on passing from C–S···Nu to N–S···Nu fragments due to the larger electronegativity of N as compared to C. The distribution of the involved distances around the mean values is broader than that of the carbon analogues as showed by the scatterplots of S···Nu *vs.* N–S distances represented in Figure 16.5 for Nu = N (a), Ch (b), and Ha (c).

The mean values calculated for the N–S and S···Nu distances in the fragments N–S···Nu are summarized in Table 16.2, along with the mean of $\delta_{N–S}$ and $\delta_{S···Nu}$ values. Figure 16.6 shows the scatterplots of $\delta_{N–S}$ *vs.* $\delta_{S···Nu}$.

The scatterplots clearly show that the relative N–S elongation values, expressed as $\delta_{N–S}$, mainly fall in a range between 2% and 10%, with a prevalence of the fragments C–S···O in the upper 8–10% range.

The $\delta_{S···Nu}$ values decrease in the order Cl ≈ O < Br < F < N < S < Se < I. The remarkable shortenings with respect to the sum of relevant vdW radii observed in those systems where the ChB donor interacts with Cl, Br, and F acceptors is strongly dependent on the presence of numerous systems featuring anionic halides as Nu.

16.2.1.3 O–S···Nu

A number of 1101 linear O–S···Nu fragments can be found in the CSD with a prevalence of O–S···O systems (836, 76%), followed in occurrence by O–S···Cl (101, 9.2%) and O–S···F (71, 6.4%) moieties.[19] Less frequent are fragments of the type O–S···N (36, 3.3%) and O–S···S (29, 2.6%), with only very few examples for Nu = Se, Te, and I. The compounds comprised in this category mainly belong to the class of sulfoxides and alkyl derivatives thereof, thiophene, sulfate, sulfite, and dithionite anions.

The mean distances calculated within the fragments O–S···Nu in the three sub-categories with Nu = N, Ch, and Ha display similar values [$d_{O–S}$ = 1.513 (0.04), 1.519 (0.05), and 1.525 (0.05) Å, $d_{S···Nu}$ = 3.27 (0.07), 3.20 (0.17), and 3.32 (0.30) Å for Nu = N, Ch, and Ha, respectively]. The O–S···Nu fragments show the covalent O–S distances falling in ranges tighter than those found in the analogous C–S···Nu and N–S···Nu fragments because of the very large number of ChB donors sporting a double bond S=O. The non-covalent S···Nu distances fall in ranges similar to those previously described and, similarly to the C–S···Nu scatterplots (Figure 16.3) well defined areas are

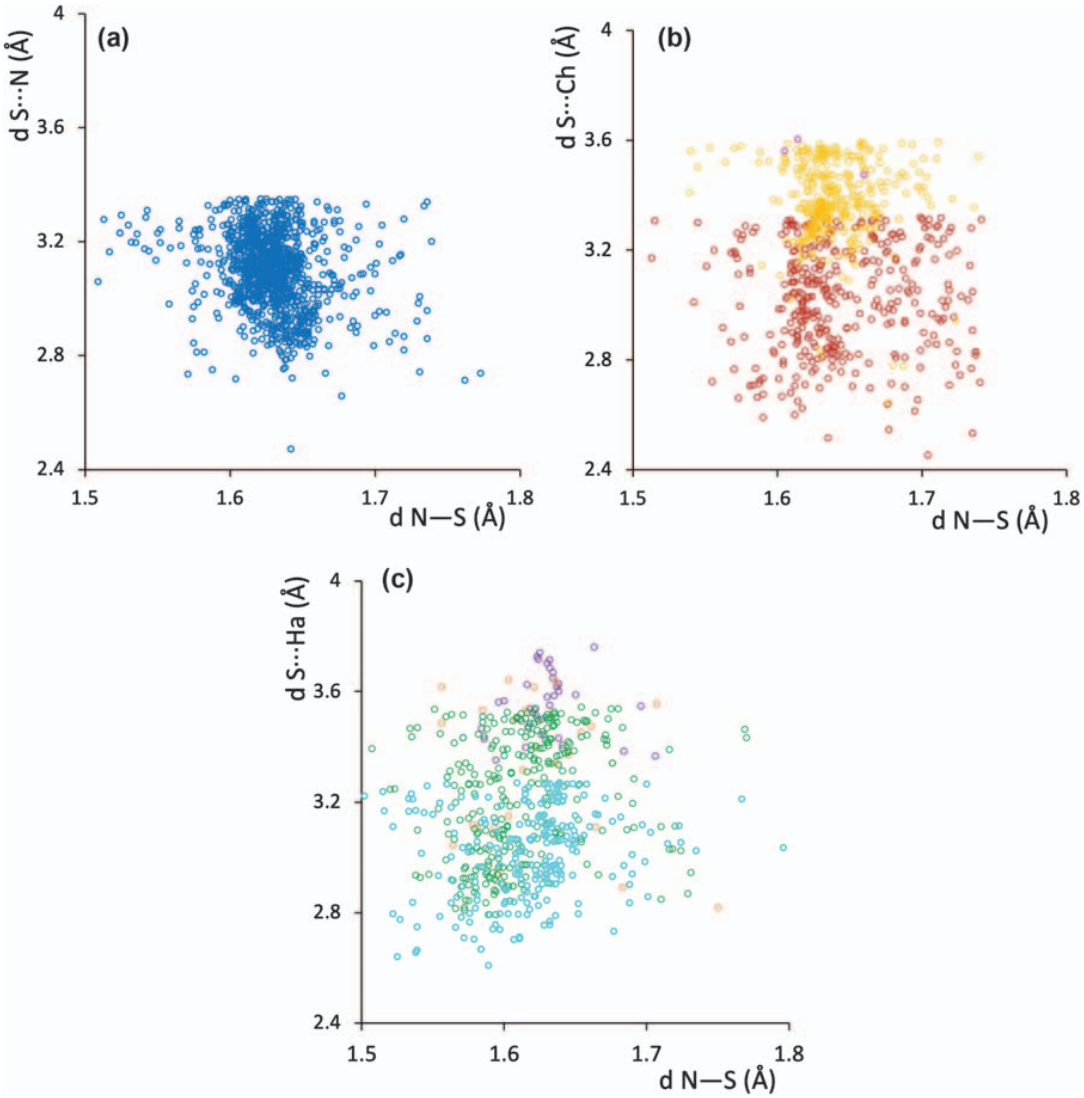

Figure 16.5 Scatterplots of $d_{S\cdots Nu}$ *vs.* $d_{N\text{–}S}$ distances in the N–S···Nu fragments for Nu = N (a); Ch (b); Ha (c). Nu colour codes: N = blue in (a); O = red, S = yellow, Se = magenta in (b); F = cyan, Cl = green, Br = orange, I = violet in (c).

Table 16.2 Occurrence, mean distances d [Å] (standard deviation, s), and δ values for N–S···Nu fragments.

Nu	Occurrence	$d_{N\text{–}S}$ (s)	$d_{S\cdots Nu}$ (s)	$\delta_{N\text{–}S}$ (%)	$\delta_{S\cdots Nu}$ (%)
O	363	1.644 (0.04)	3.017 (0.21)	3.16	− 9.13
S	341	1.639 (0.03)	3.375 (0.21)	4.42	− 6.25
Se	3	1.626 (0.03)	3.545 (0.07)	3.83	− 4.18
N	1116	1.629 (0.03)	3.099 (0.13)	4.70	− 7.48
Br	27	1.622 (0.05)	3.329 (0.25)	2.60	− 8.81
Cl	297	1.613 (0.04)	3.222 (0.22)	3.34	− 9.24
F	244	1.615 (0.05)	3.001 (0.21)	3.03	− 8.22
I	35	1.630 (0.03)	3.559 (0.12)	4.33	− 5.85

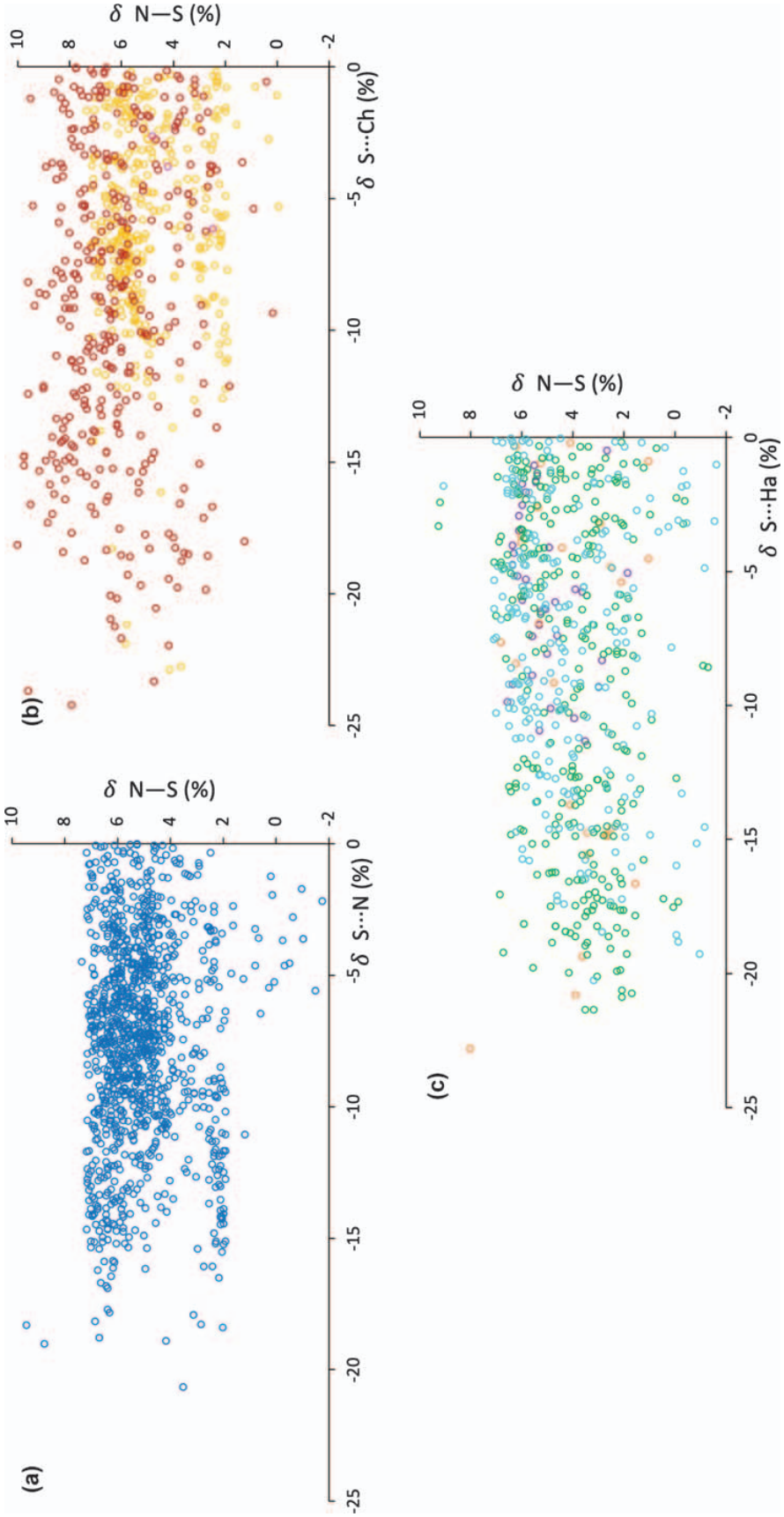

Figure 16.6 Scatterplots of $\delta_{N\text{-}S}$ *vs.* $\delta_{S\cdots Nu}$ calculated for the N–S···Nu fragments for Nu = N (a); Ch (b); Ha (c). Nu colour codes: N = blue in (a); O = red, S = yellow, Se = magenta in (b); F = cyan, Cl = green, Br = orange, I = violet in (c).

recognizable for the different acceptor atoms Nu involved in the interaction (Figure 16.7).

The mean values calculated for the O–S and S···Nu distances in the fragments O–S···Nu are summarized in Table 16.3, along with the mean of δ_{O-S} and $\delta_{S\cdots Nu}$ calculated values. Figure 16.8 shows the scatterplots of δ_{O-S} *vs.* $\delta_{S\cdots Nu}$.

The scatterplot in Figure 16.8 clearly shows a small range of values covered by the relative O–S elongations, expressed as δ_{O-S}, mainly falling in a range between −2% and 2% for all the fragments, indicating a very weak nature for these ChB interactions. Fragments O–S···O and O–S···F show values in the range from −7% and 7%, and stronger CHBs, as confirmed by the decreasing of $\delta_{S\cdots Nu}$ values in the order F < O < Cl < S < N < Br < I.

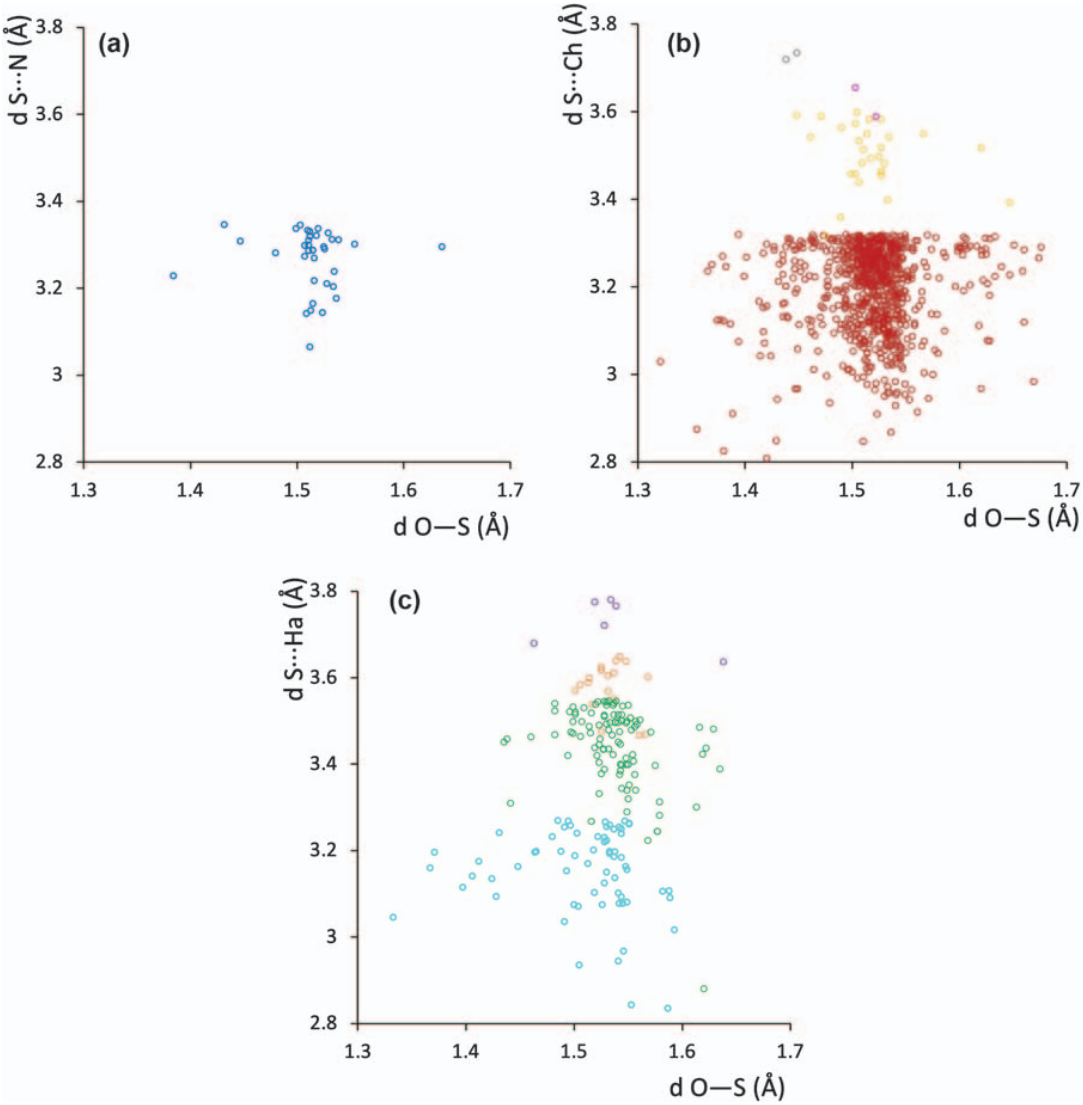

Figure 16.7 Scatterplots of $d_{S\cdots Nu}$ *vs.* d_{O-S} distances in the O–S···Nu fragments for Nu = N (a); Ch (b); Ha (c). Nu colour codes: N = blue in (a); O = red, S = yellow, Se = magenta, Te = black in (b); F = cyan, Cl = green, Br = orange, I = violet in (c).

Table 16.3 Occurrence, mean distances d [Å] (standard deviation, s), and δ values for O–S···Nu fragments.

Nu	Occurrence	$d_{O–S}$ (s)	$d_{S\cdots Nu}$ (s)	$\delta_{O–S}$ (%)	$\delta_{S\cdots Nu}$ (%)
O	836	1.519 (0.05)	3.183 (0.16)	0.311	− 4.12
S	29	1.518 (0.04)	3.500 (0.07)	0.129	− 2.77
Se	2	1.512 (0.01)	3.622 (0.05)	0.166	− 2.12
Te	2	1.443 (0.007)	3.727 (0.01)	− 4.44	− 3.45
N	36	1.513 (0.04)	3.268 (0.07)	0.212	− 2.46
Br	18	1.532 (0.02)	3.578 (0.06)	1.49	− 1.97
Cl	101	1.537 (0.04)	3.429 (0.16)	1.38	− 3.41
F	71	1.505 (0.06)	3.075 (0.3)	− 0.041	− 5.95
I	6	1.537 (0.06)	3.727 (0.06)	0.87	− 1.41

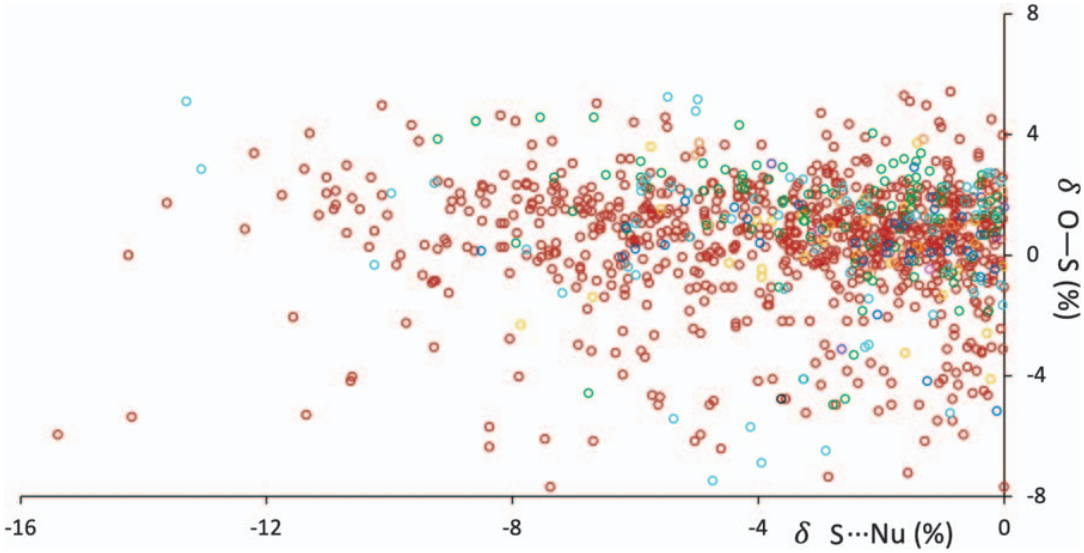

Figure 16.8 Scatterplot of $\delta_{O–S}$ *vs.* $\delta_{S\cdots Nu}$ calculated for the O–S···Nu fragments. Nu colour codes: N = blue, O = red, S = yellow, Se = magenta, Te = black, F = cyan, Cl = green, Br = orange, I = violet.

16.2.1.4 S–S···Nu

Deposited at the CSD are 1602 linear S–S···Nu fragments, including S–S···N (180, 11.3%), S–S···Ch (845, 52.7%), and S–S···Ha (577, 36.0%) moieties.[19] Belonging to this category are ChB donors such as disulfides and polysulfides, tetrathiocines, thiosulfate anions, and dithia-cyclic and polycyclic derivatives.

The mean distances calculated within the fragments S–S···Nu in the three sub-categories with Nu = N, Ch, and Ha display the covalent S–S distances varying in a very narrow range with values of the non-covalent S···Nu interactions falling in ranges close to those previously described [$d_{S–S}$ = 2.086 (0.04), 2.060 (0.05), and 2.051 (0.04) Å; $d_{S\cdots Nu}$ = 3.14 (0.12), 3.33 (0.20), and 3.20 (0.22) Å for Nu = N, Ch, and Ha, respectively]. Figure 16.9 reports the scatterplots of $d_{S\cdots Nu}$ *vs.* $d_{S–S}$ distances for Nu = N (a), Ch (b), and Ha (c) displaying similar values for the different ChB acceptor sub-categories.

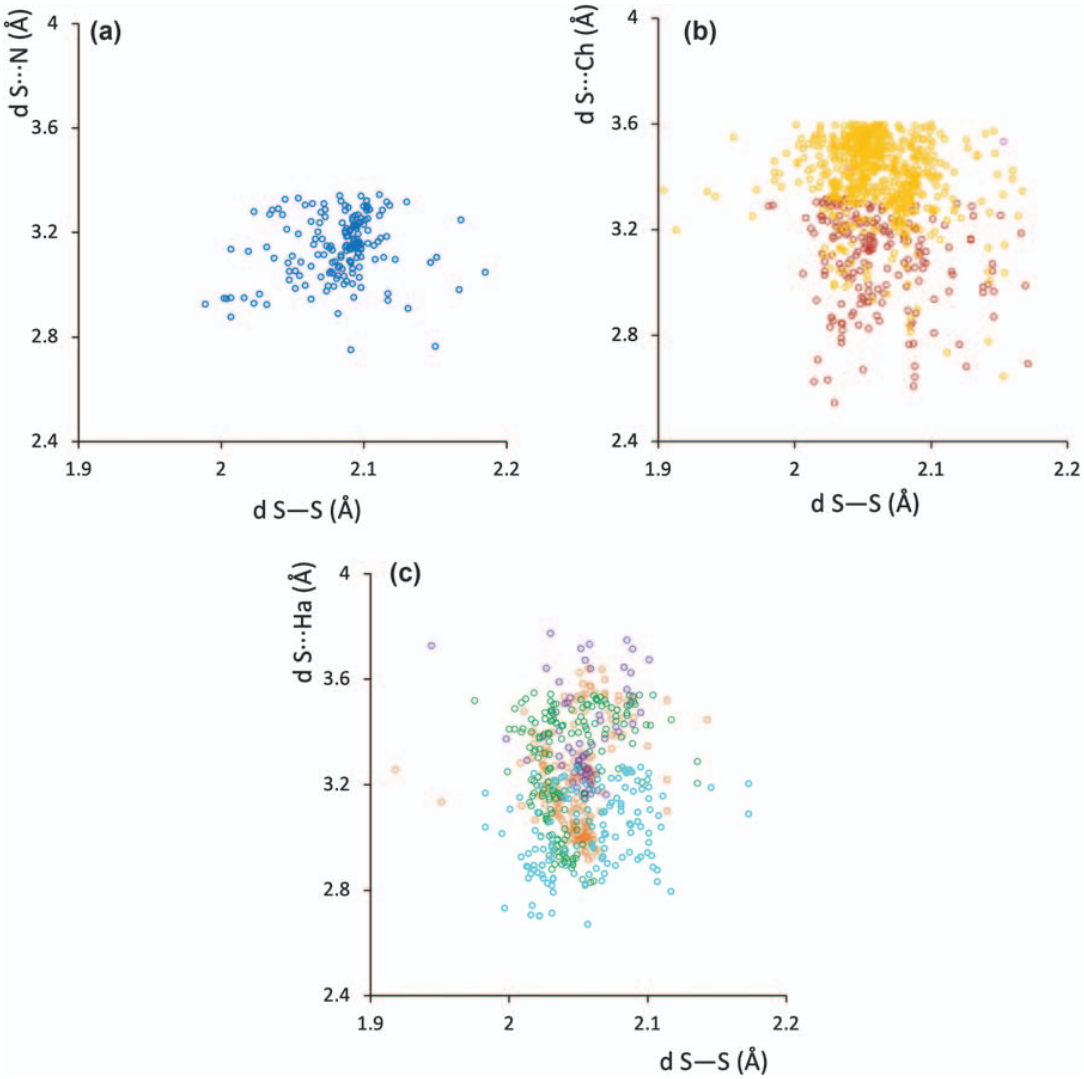

Figure 16.9 Scatterplots of $d_{S\cdots Nu}$ *vs.* d_{S-S} distances in the S–S···Nu fragments for Nu = N (a), Ch (b); Ha (c). Nu colour codes: N = blue in (a); O = red, S = yellow, Se = magenta in (b); F = cyan, Cl = green, Br = orange, I = violet in (c).

The mean values calculated for the S–S and S···Nu distances in the fragments S–S···Nu are summarized in Table 16.4, along with the mean of δ_{S-S} and $\delta_{S\cdots Nu}$ values calculated as described above (eqn (16.1) and (16.2)); Figure 16.10 shows the scatterplots of δ_{S-S} *vs.* $\delta_{S\cdots Nu}$.

The scatterplots clearly confirm the small range of values covered by the relative S–S elongations, expressed as δ_{S-S}, mainly falling in a range between −2% and 4%.

The $\delta_{S\cdots Nu}$ values show a decrease in the order Br < I < Cl < F < < O < N < S, showing that the stronger ChBs involve Nu = Ha. This trend can be probably explained taking into account that 72% of the compounds involved in S–S···Ha ChB interactions are salts where cations featuring the S–S moieties interact with the halide counterions.

Table 16.4 Occurrence, mean distances d [Å] (standard deviations s), and δ values for S–S···Nu fragments.

Nu	Occurrence	$d_{S–S}$ (s)	$d_{S\cdots Nu}$ (s)	$\delta_{S–S}$ (%)	$\delta_{S\cdots Nu}$ (%)
O	199	2.062 (0.04)	3.086 (0.18)	1.09	− 7.05
S	642	2.059 (0.05)	3.401 (0.15)	0.918	− 5.54
Se	4	2.066 (0.06)	3.372 (0.11)	1.29	− 8.87
N	180	2.086 (0.04)	3.144 (0.12)	2.27	− 6.14
Br	186	2.049 (0.03)	3.203 (0.16)	0.45	− 12.25
Cl	177	2.046 (0.04)	3.269 (0.21)	0.27	− 7.92
F	145	2.060 (0.04)	3.027 (0.13)	0.966	− 7.42
I	69	2.054 (0.02)	3.384 (0.15)	0.691	− 10.47

16.2.2 R–Se···Nu fragments

A total number of 4109 linear fragments R–Se···Nu (R = B, C, N, P, As, O, S, Se, Te and Nu = N, P, As, Sb, O, S, Se, Te, F, Cl, Br, I) can be found to date in the CSD, notably lower than that recorded for the fragments containing the lighter congener S.[19] The following survey is limited to the same categories of fragments considered in the previous section (R = C, N, O, and S) with the addition of ChB donors featuring a Se–Se moiety, isologue to the S–S one discussed in the previous section. The histogram plot in Figure 16.11 shows the occurrence of fragments R–Se···Nu sorted by R and Nu, with a net prevalence of C–Se···Nu systems (2363, 57.5%), followed by N–Se···Nu (573, 13.9%), Se–Se···Nu (504, 12.3%), O–Se···Nu (220, 5.3%), and S–Se···Nu (97, 2.4%) fragments. The contribution coming from different systems that globally contributes to the 8.6% of the total fragments is very heterogeneous and remains untapped by this review.

16.2.2.1 C–Se···Nu

A number of 2363 C–Se···Nu linear fragments were found in the CSD; among them, 56.2% are C–Se···Ch systems involving ChB acceptors featuring nucleophile ChB-acceptors featuring a chalcogen Lewis donor atom;[19] the remaining fragments are of the type C–Se···Ha (32.2%) and C–Se···N (11.6%). No fragments with Nu = Pn different from N were found with the only exception of 1 fragment coming from a P–Se heterocycle based on peri-substituted naphthalene.[22]

The compounds comprised in this survey are isologues to those considered in Section 16.3.1.1 and belong to the classes of selenium-containing heterocycles such as selenophene and selenaazole, selenafulvalene derivatives, selenocarbamates, selenoureas, selenoxides, selenocyanates, selenoethers, and selenium-containing macrocycles.

AQ:1

The number of linear fragments C–Se···Ch amounts to 1329, with a net prevalence for ChB-acceptors featuring selenium (C–Se···Se 54%) and oxygen (C–Se···O 32%) as Nu interacting atoms, in analogy with what was found for the C–S···Ch items. The fragments C–Se···Ha involving ChB-acceptors interacting through halogen atoms are 761 (C–Se···F, 22.5%; C–Se···Cl,

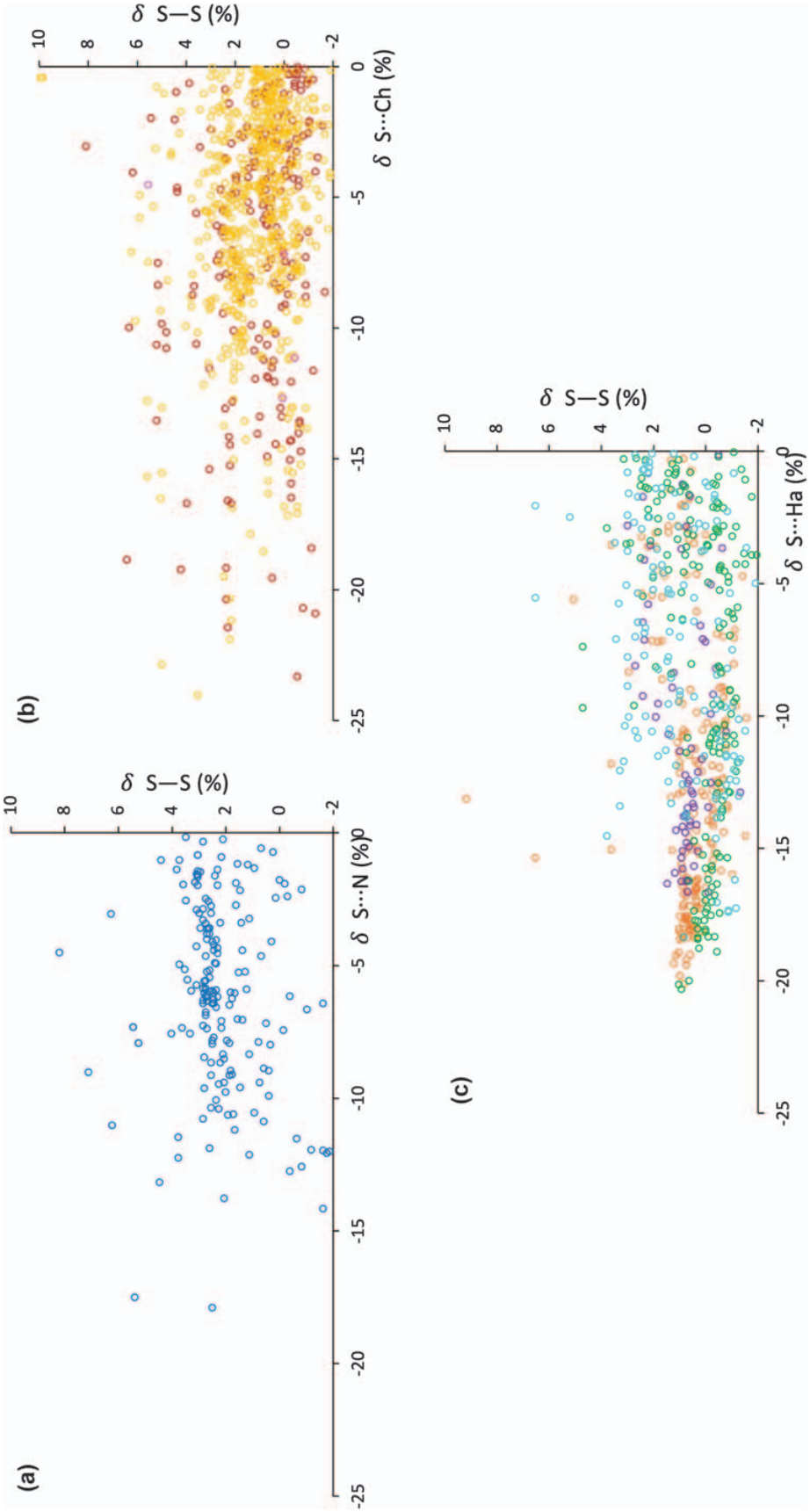

Figure 16.10 Scatterplots of $\delta_{S\text{-}S}$ *vs.* $\delta_{S\cdots Nu}$ calculated for the S–S···Nu fragments for Nu = N (a); Ch (b); Ha (c). Nu colour codes: N = blue in (a); O = red, S = yellow, Se = magenta in (b), F = cyan, Cl = green, Br = orange, I = violet in (c).

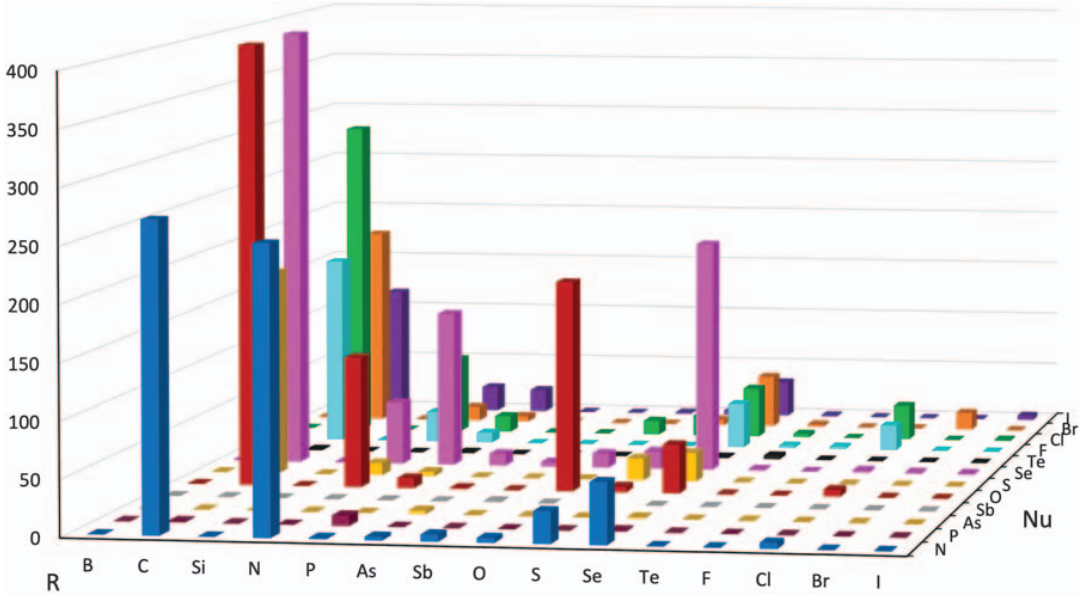

Figure 16.11 Linear R–Se···Nu fragment occurrence (R = B, C, Si, N, P, As, Sb, O, S, Se, Te, F, Cl, Br, I; Nu = N, P, As, Sb, O, S, Se, Te, F, Cl, Br, I) deposited at the CSD.

38.4%; C–Se···Br, 23.9%; C–Se···I, 15.2%), while those involving N-acceptors (C–Se···N) are 272. The mean covalent and non-covalent bond distances calculated within the fragments C–Se···Nu are roughly independent on the nature of Nu [$d_{C-Se} = 1.883$ (0.05), 1.899 (0.05), and 1.910 (0.04) Å, and $d_{S\cdots Nu} = 3.19$ (0.16), 3.46 (0.26), and 3.43 (0.21) Å, for Nu = N, Ch, and Ha, respectively]. Taking into account the different values of S and Se covalent and vdW radii, the mean distances found in C–Se···Nu fragments are comparable with those found in the analogous sulfur fragments as confirmed by the range of existence showed in scatterplots of Se···Nu *vs.* C–Se distances for Nu = N (a), Ch (b), and Ha (c) reported in Figure 16.12. This notwithstanding, probably due to the larger polarizability of Se with respect to S, wide distributions of the values can be noticed, especially for the C–Se···Ha systems (Figure 16.12c).

The mean values calculated for the C–Se and Se···Nu distances in the fragments C–Se···Nu are summarized in Table 16.5, along with the mean of δ_{C-Se} and $\delta_{Se\cdots Nu}$ values, calculated as explained above (eqn (16.1) and (16.2)). Figure 16.13 shows the scatterplots of δ_{C-Se} *vs.* $\delta_{Se\cdots Nu}$.

The scatterplots show relative C–Se elongations, expressed as δ_{C-Se}, varying in a range between 0% and 13%. Akin to what was previously observed for the C–S···Nu fragments, three main bands of data can be identified in the scatterplots depending on the nature of the molecule engaged in the ChB: selenocyanates, selenafulvalene derivatives, and selenium-heterocyclic compounds show evident elongations δ_{C-Se}, whilst systems with the selenium atom directly bound to different electron-donating substituents show shorter elongations with some negative values corresponding to systems involved in very weak ChBs, such as in the case of dialkyl selenoxides.

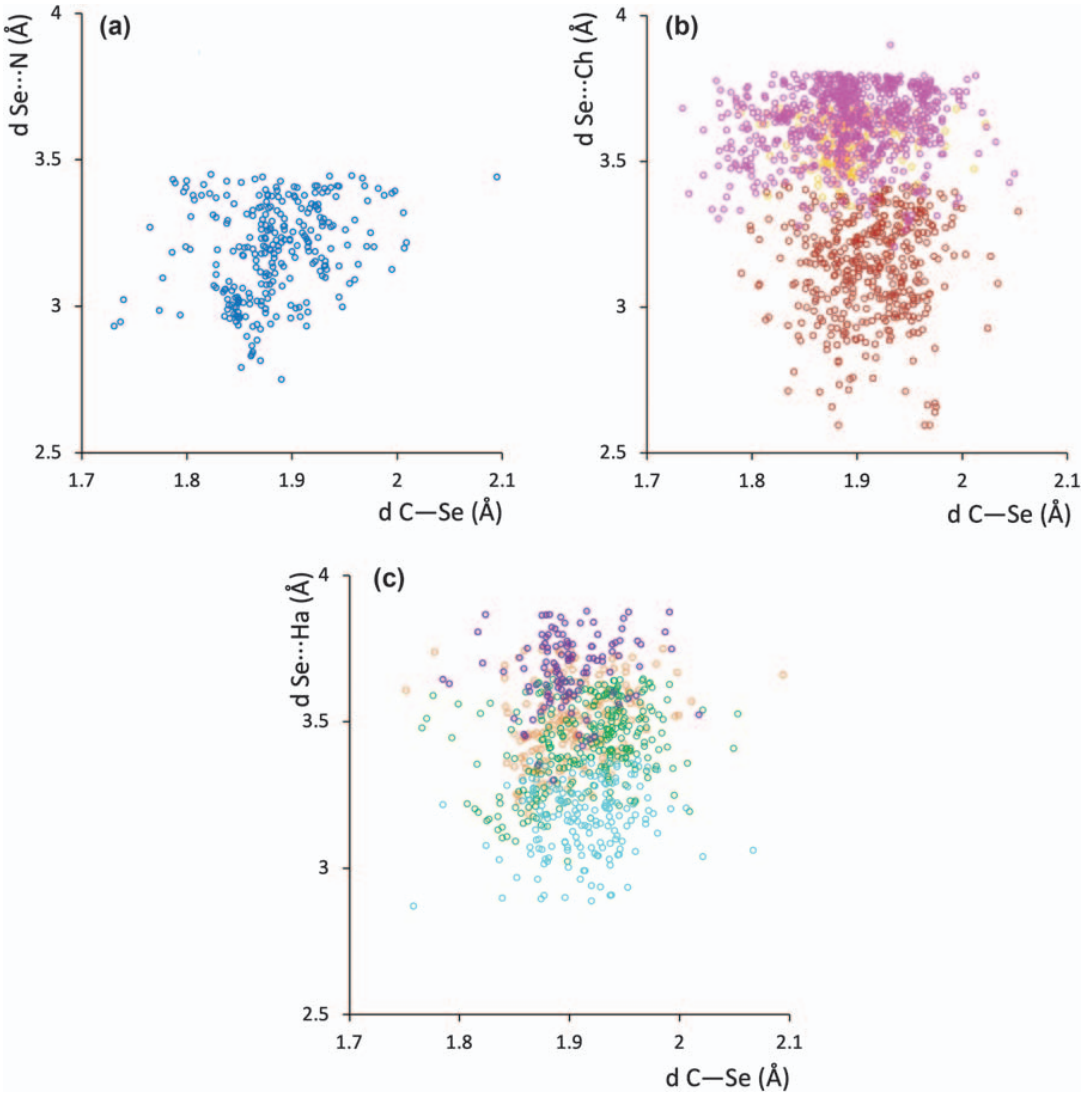

Figure 16.12 Scatterplots of $d_{Se\cdots Nu}$ *vs.* d_{C-Se} distances in the C–Se···Nu fragments for Nu = N (a); Ch (b); Ha (c). Nu colour codes: N = blue in (a); O = red, S = yellow, Se = magenta in (b); F = cyan, Cl = green, Br = orange, I = violet in (c).

Table 16.5 Occurrence, mean distances d [Å] (standard deviation, s), and δ values for C–Se···Nu fragments.

Nu	Occurrence	d_{C-Se} (s)	$d_{Se\cdots Nu}$ (s)	δ_{C-Se} (%)	$\delta_{Se\cdots Nu}$ (%)
O	424	1.912 (0.05)	3.137 (0.18)	6.57	− 8.19
S	186	1.891 (0.03)	3.560 (0.08)	7.07	− 4.20
Se	718	1.893 (0.06)	3.629 (0.12)	4.34	− 4.43
N	273	1.883 (0.05)	3.189 (0.16)	6.79	− 7.61
Br	182	1.905 (0.05)	3.498 (0.13)	6.12	− 6.71
Cl	292	2.053 (0.05)	3.427 (0.14)	4.26	− 6.10
F	171	1.913 (0.04)	3.167 (0.12)	4.07	− 6.03
I	116	1.900 (0.04)	3.682 (0.12)	6.36	− 5.11

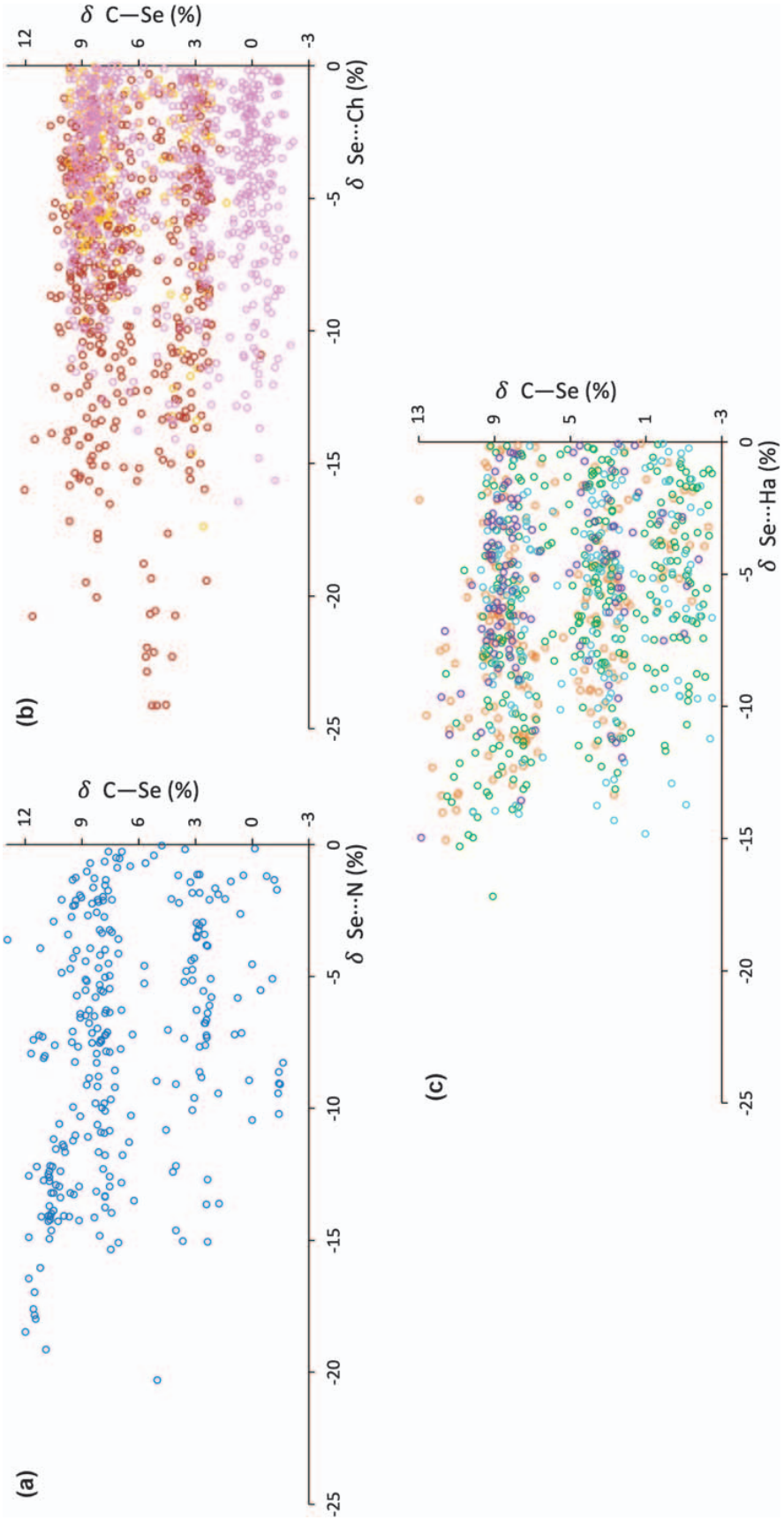

Figure 16.13 Scatterplots of δ_{C-Se} *vs.* $\delta_{Se\cdots Nu}$ calculated for the C–Se· · ·Nu fragments for Nu = N (a); Ch (b); Ha (c). Nu colour codes: N = blue in (a); O = red, S = yellow, Se = magenta in (b); F = cyan, Cl = green, Br = orange, I = violet in (c).

The strength of the ChB, defined by the $\delta_{Se\cdots Nu}$ value follows the order O < N < Br < Cl < F < I < Se with increased shortenings with respect to the C–S···Nu isologues, confirming the expected strengthening of the ChB on passing from S to Se. The trend cannot be clearly related to any simple property of the nucleophile Lewis donor atom Nu, thus suggesting that the nature of the interaction, and hence the relative contributions of the electrostatic and CT terms, vary along the series.

16.2.2.2 N–Se···Nu

The number of linear Pn–Se···Nu fragments identified in the CSD amounts to 817,[19] but only those with a N–Se covalent bond (573 items, 70%) will be analyzed here in analogy to the choice adopted for the sulfur isologues reported in Section 16.3.1.2. In fact, the compounds encompassed are usually the corresponding Se-analogous of the previously described S-isologues, *i.e.*, selenenyl amide derivatives and Se-containing heterocycles such as selenophene and selenazoles and the fused polycyclic derivative thereof. Among the linear N–Se···Nu fragments can be identified 253 (44.1%) N–Se···N, 186 (32.5%) N–Se···Ch, and 134 (23.4%) N–S···Ha moieties. The mean N–Se and Se···Nu distances calculated for the three sub-categories with Nu = N, Ch, and Ha display similar values [d_{N-Se} = 1.800 (0.04), 1.827 (0.04), and 1.798 (0.05) Å; $d_{Se\cdots Nu}$ = 3.19 (0.16), 3.46 (0.26), and 3.42 (0.21) Å, for Nu = N, Ch, and Ha, respectively]. As observed for the isologues with sulfur, N–Se···Nu fragments show covalent N–Se and non-covalent Se···Nu distances notably shorter than those found in the analogous C–Se···Nu fragments, notwithstanding the similar values of the covalent and vdW radii of the involved atoms, confirming the expected strengthening of the ChB on passing from C–Se···Nu to N–Se···Nu fragments. The distribution of the involved distances around the mean values is broad as showed by the scatterplots of Se···Nu *vs.* N–Se distances presented in Figure 16.14 for Nu = N (a), Ch (b), and Ha (c).

In fact, the Se···Nu mean distances are shorter than the corresponding S···Nu ones, notwithstanding the larger Se vdW radium, and the means of the normalized shortening $\delta_{Se\cdots Nu}$ are almost doubled passing from −9.13% to −16.47% and from −7.48% to −14.65% for Nu = O and N, just to make the examples for the high-frequently occurring fragments (Tables 16.2 and 16.6).

The scatterplots of δ_{N-Se} *vs.* $\delta_{Se\cdots Nu}$ (Figure 16.15) confirm an amplified shortening with numerous fragments showing $\delta_{Se\cdots Nu}$ distances falling in the range from −15% to −30%.

16.2.2.3 O–Se···Nu

A search in the CSD reveals 220 linear O–Se···Nu fragments with a large prevalence of systems featuring a chalcogen as the ChB acceptor (O–Se···O, 86%; O–Se···Se, 6%, O–Se···Cl, 6%, and O–Se···N, 2%).[19] The compounds comprised in this category mainly belong to the class of selenite and selenate anions, selenoxides, and derivatives thereof.

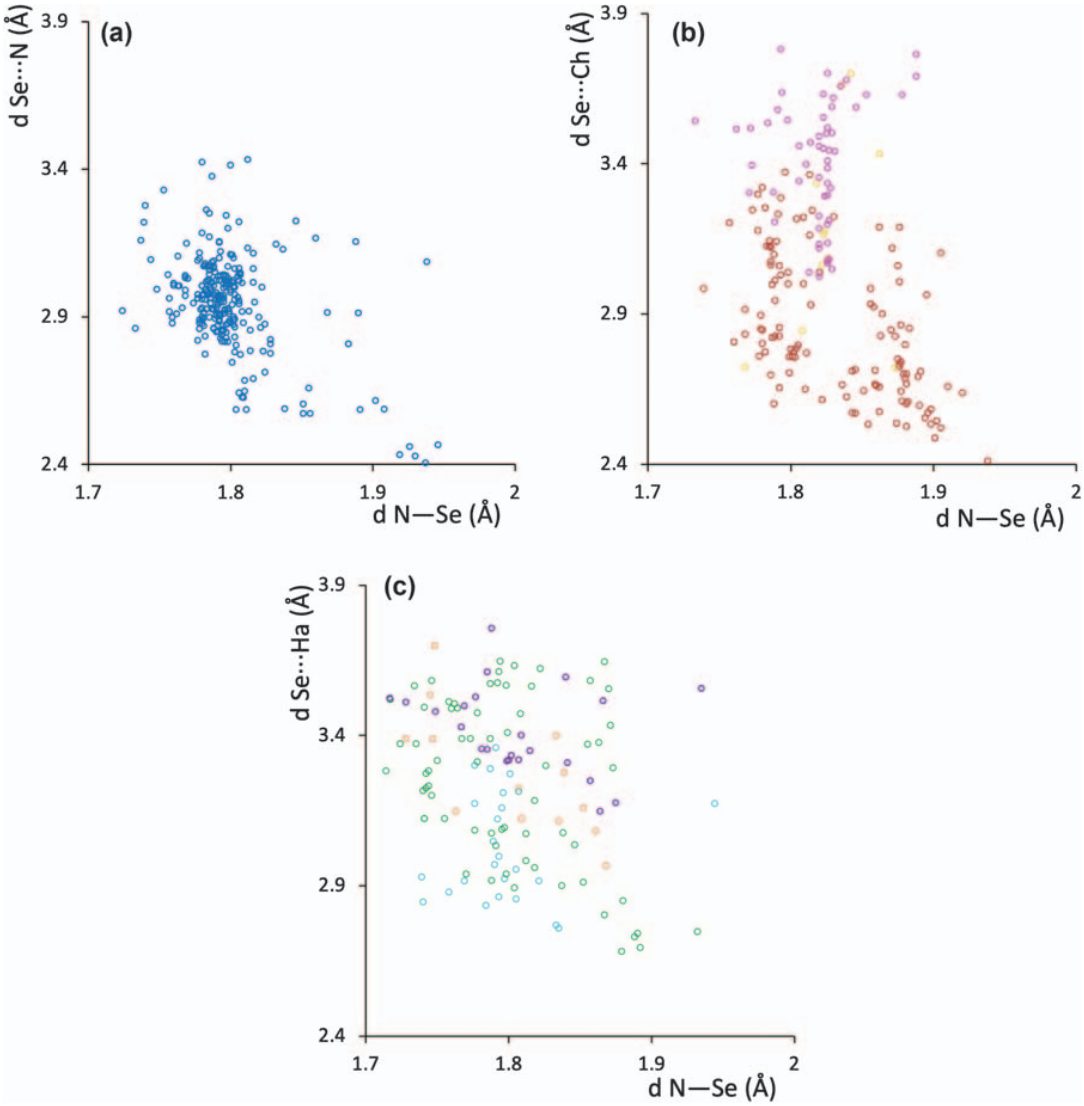

Figure 16.14 Scatterplots of $d_{Se\cdots Nu}$ *vs.* d_{N-Se} distances in the N–Se···Nu fragments for Nu = N (a); Ch (b); Ha (c). Nu colour codes: N = blue in (a); O = red, S = yellow, Se = magenta in (b); F = cyan, Cl = green, Br = orange, I = violet in (c).

Table 16.6 Occurrence, mean distances d [Å] (standard deviation, s), and δ values for N–Se···Nu fragments.

Nu	Occurrence	d_{N-Se} (s)	$d_{Se\cdots Nu}$ (s)	δ_{N-Se} (%)	$\delta_{Se\cdots Nu}$ (%)
O	118	1.832 (0.05)	2.857 (0.23)	2.75	− 16.47
S	11	1.827 (0.03)	3.174 (0.34)	6.25	− 14.22
Se	57	1.816 (0.03)	3.412 (0.20)	7.71	− 10.22
N	253	1.800 (0.04)	2.945 (0.17)	5.89	− 14.65
Br	13	1.803 (0.05)	3.270 (0.20)	4.14	− 12.81
Cl	70	1.800 (0.06)	3.254 (0.27)	4.31	− 10.85
F	28	1.785 (0.05)	3.003 (0.19)	4.91	− 10.88
I	23	1.807 (0.05)	3.418 (0.02)	5.35	− 11.90

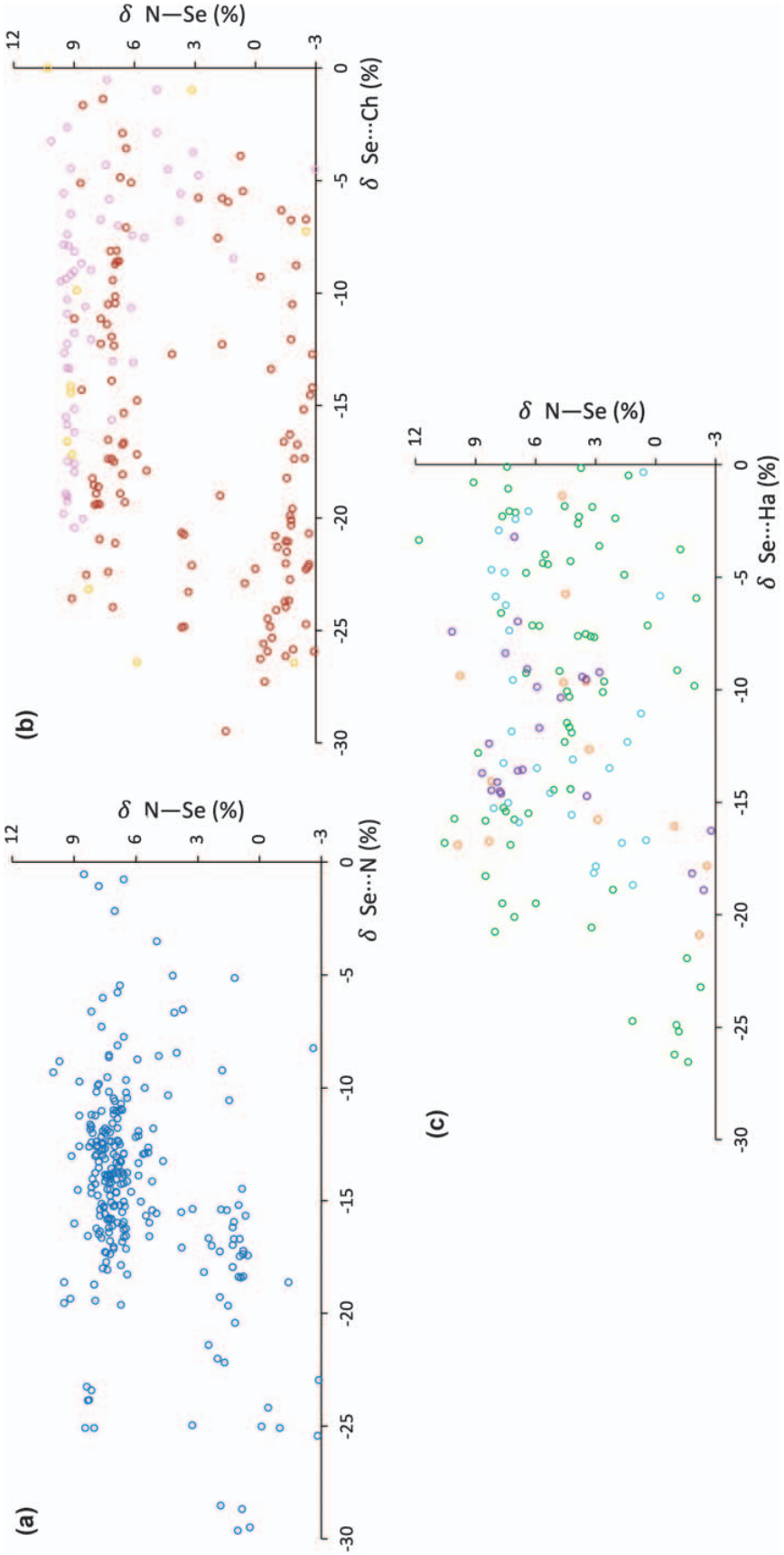

Figure 16.15 Scatterplots of $\delta_{\text{N-Se}}$ *vs.* $\delta_{\text{Se}\cdots\text{Nu}}$ calculated for the N–Se···Nu fragments for Nu = N (a); Ch (b); Ha (c). Nu colour codes: N = blue in (a); O = red, S = yellow, Se = magenta in (b); F = cyan, Cl = green, Br = orange, I = violet in (c).

Table 16.7 Occurrence, mean distances d [Å] (standard deviation, s), and δ values for O–Se···Nu fragments.

Nu	Occurrence	$d_{O–Se}$ (s)	$d_{Se\cdots Nu}$ (s)	$\delta_{O–Se}$ (%)	$\delta_{Se\cdots Nu}$ (%)
O	189	1.734 (0.07)	3.028 (0.24)	2.00	− 11.45
Se	13	1.740 (0.07)	3.621 (0.10)	2.22	− 4.71
N	4	1.721 (0.16)	3.252 (0.19)	2.00	− 5.74
Cl	13	1.697 (0.09)	3.378 (0.14)	4.74	− 7.45

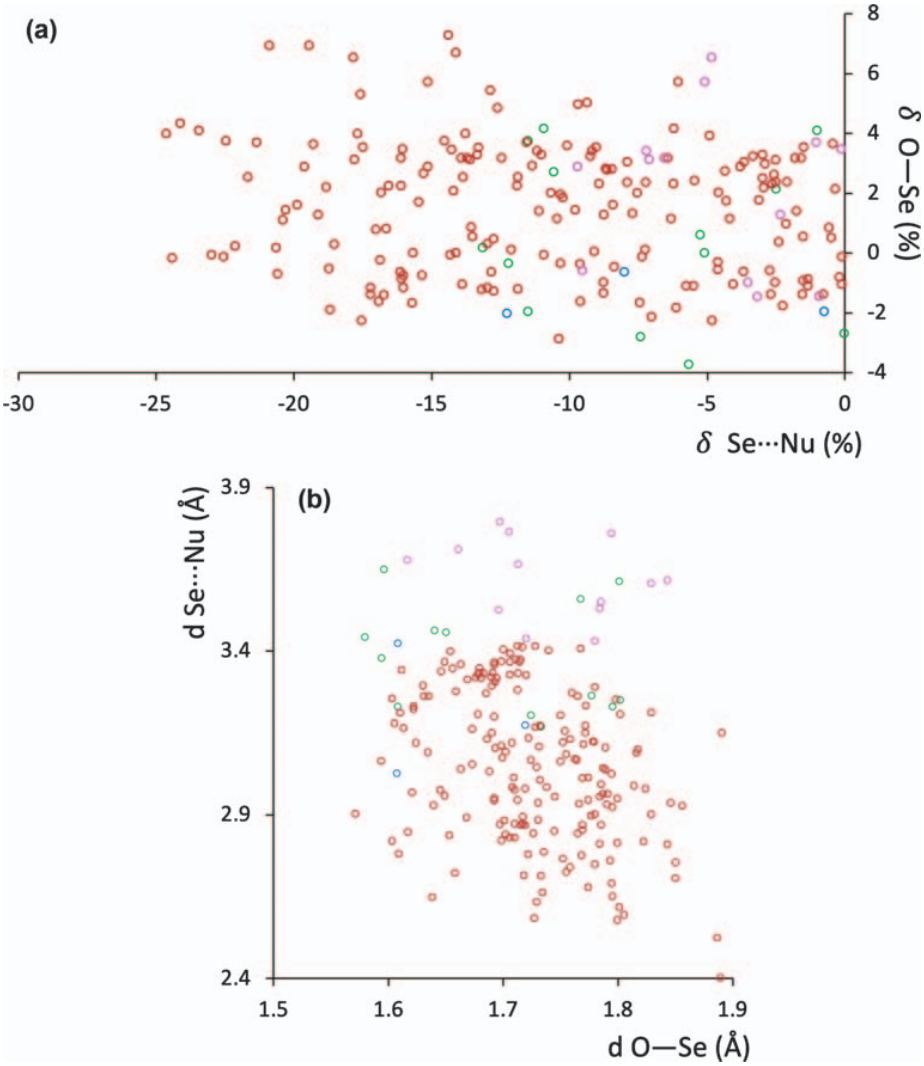

Figure 16.16 Scatterplots of $\delta_{O–Se}$ *vs.* $\delta_{Se\cdots Nu}$ (a) and $d_{Se\cdots Nu}$ *vs.* $d_{O–Se}$ (b) for the O–Se···Nu fragments. Nu colour codes: N = blue, O = red, Se = magenta, Cl = green.

The mean values calculated for the O–Se and Se···Nu distances in the fragments O–S···Nu are summarized in Table 16.7, along with the mean of $\delta_{O–Se}$ and $\delta_{Se\cdots Nu}$ values. Figure 16.16 shows the scatterplots of $\delta_{O–Se}$ *vs.* $\delta_{Se\cdots Nu}$ values (a), and Se···Nu *vs.* O–Se distances (b). The fragments typically show short covalent O–Se and non-covalent Se···Nu distances mainly falling in the range 1.6–1.8 and 2.6–3.6 Å, respectively, following a tendency similar to that evidenced for the O–S···Nu fragments. The strength of the involved

ChBs is increased with respect to the lighter S-isologues with the stronger interactions involving O and Cl, as the ChB acceptors.

16.2.2.4 S–Se···Nu

The number of linear S–Se···Nu fragments amounts to 97, with Nu = N (29%), Ch (42%), and Ha (29%).[19] The compounds comprised in this group belong to the same classes examined in Section 16.3.1.4, with a selenium atom replacing a sulfur one, such as thiaselenazoles, selanyl-sulfanyl, thiaselane, and selenol derivatives.

The mean distances calculated within the fragments S–Se···Nu does not significantly depend on the nature of Nu, and therefore present very close values for Nu = N, Ch, and Ha [$d_{S–Se}$ = 2.234 (0.05), 2.222 (0.03), and 2.219 (0.06) Å; $d_{Se···Nu}$ = 2.84 (0.25), 3.36 (0.26), and 3.16 (0.17) Å for Nu = N, Ch, and Ha, respectively]. As shown in Figure 16.17, where the scatterplots of

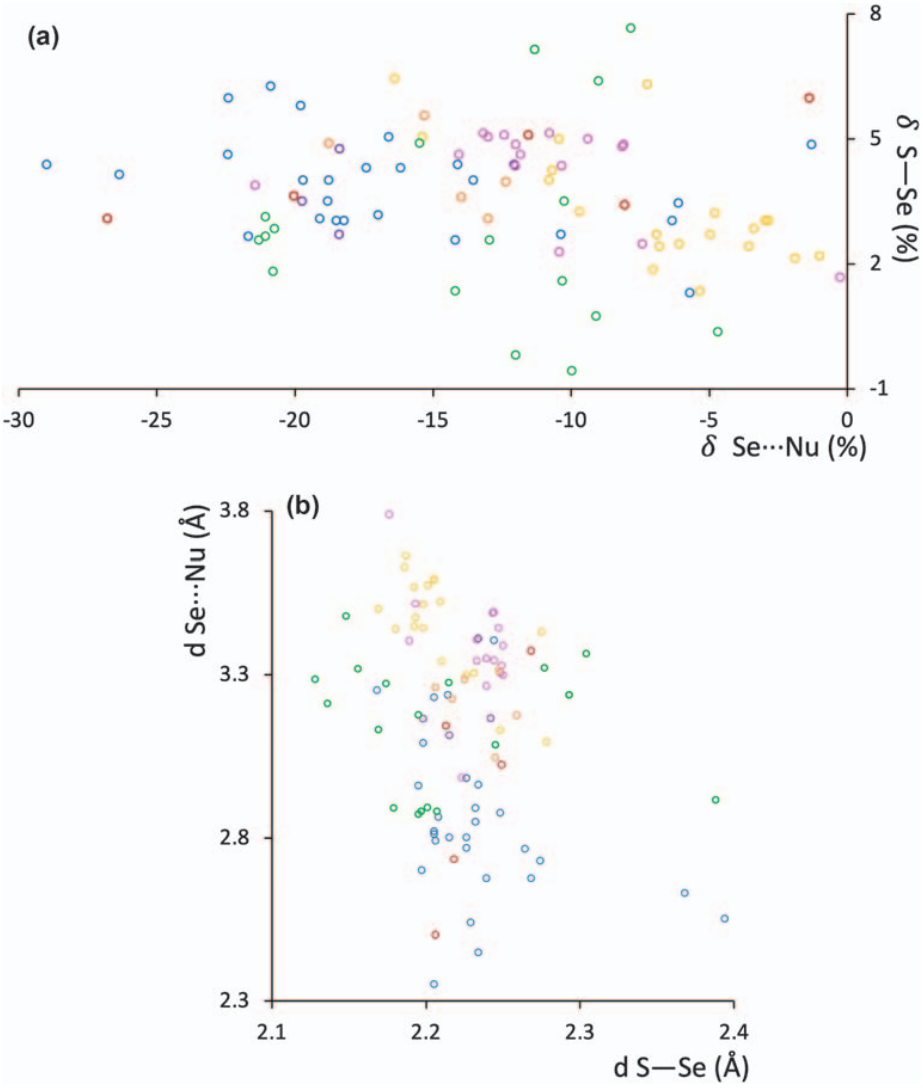

Figure 16.17 Scatterplots of $\delta_{S–Se}$ *vs.* $\delta_{Se···Nu}$ (a) and $d_{Se···Nu}$ *vs.* $d_{S–Se}$ (b) for the S–Se···Nu fragments. Nu colour codes: N = blue, O = red, S = yellow, Se = magenta, Cl = green, Br = orange, I = violet.

Table 16.8 Occurrence, mean distances d [Å] (standard deviations s), and δ values for S–Se···Nu fragments.

Nu	Occurrence	$d_{S–Se}$ (s)	$d_{Se\cdots Nu}$ (s)	$\delta_{S–Se}$ (%)	$\delta_{Se\cdots Nu}$ (%)
O	5	2.231 (0.03)	2.956 (0.34)	4.24	−13.56
S	20	2.212 (0.03)	3.444 (0.16)	3.34	−6.91
Se	16	2.231 (0.02)	3.385 (0.16)	4.26	−10.93
N	28	2.234 (0.05)	2.839 (0.24)	4.40	−17.71
Br	5	2.230 (0.02)	3.199 (0.09)	4.22	−14.69
Cl	19	2.216 (0.07)	3.144 (0.20)	3.54	−13.87
I	4	2.222 (0.02)	3.215 (0.13)	3.84	−17.15

$\delta_{S–Se}$ *vs.* $\delta_{Se\cdots Nu}$ values (a) and Se···Nu *vs.* S–Se distances (b) are reported, the covalent S–Se distances fall in a narrow range, and the Se···Nu contacts show values comparable or even shorter that those found for the S–S···Nu isologues, despite the larger vdW radius of the Se atom compared to the S one.

The mean values calculated for the S–Se and Se···Nu distances in the fragments S–Se···Nu are summarized in Table 16.8, along with the mean of $\delta_{S–Se}$ and $\delta_{Se\cdots Nu}$ values calculated as described above (eqn (16.1) and (16.2)).

The data reported in Table 16.8 and Figure 16.17a confirm the small range covered by the S–Se elongations, with $\delta_{S–Se}$ values mainly falling between 0% and 5%. As expected, the mean $\delta_{Se\cdots Nu}$ values, ranging between −18% and −7%, reveal an increase in the strength of the ChB involved, as compared to the lighter sulfur isologues.

16.2.2.5 Se–Se···Nu

The number of linear Se–Se···Nu fragments involving a ChB amounts to 504.[19] Among them, moieties with Nu = N (10.7%), Ch (55.5%), and Ha (33.3%) are found, with only a single Se–Se···P and a single Se–Se···As fragment (0.5%). Belonging to this category are compounds with a Se–Se bond such as diselenides and polyselenides, and diselena-cycles and aza-cycles derivatives.

The mean distances calculated within the fragments Se–Se···Nu in the three sub-categories with Nu = N, Ch, and Ha present very similar values for the covalent Se–Se distances [$d_{Se–Se}$ = 2.336 (0.04), 2.343 (0.06), and 2.344 (0.05) Å, for Nu = N, Ch, and Ha, respectively]. The interaction Se···Nu shows mean values as large as 3.09 (0.16), 3.41 (0.27), and 3.24 (0.25) Å for Nu = N, Ch, and Ha, respectively, in line with the other R–Se···Nu systems. Figure 16.18 reports the scatterplots of Se···Nu *vs.* Se–Se distances for Nu = N (a), Ch (b), and Ha (c) showing spread regions of existence of fragments involving different acceptors without any loss of continuity.

The mean values calculated for the Se–Se and Se···Nu distances in the fragments Se–Se···Nu along with the mean values of the pertinent $\delta_{Se–Se}$ and $\delta_{Se\cdots Nu}$ are summarized in Table 16.9. Figure 16.19 shows the scatterplots of $\delta_{Se–Se}$ *vs.* $\delta_{Se\cdots Nu}$.

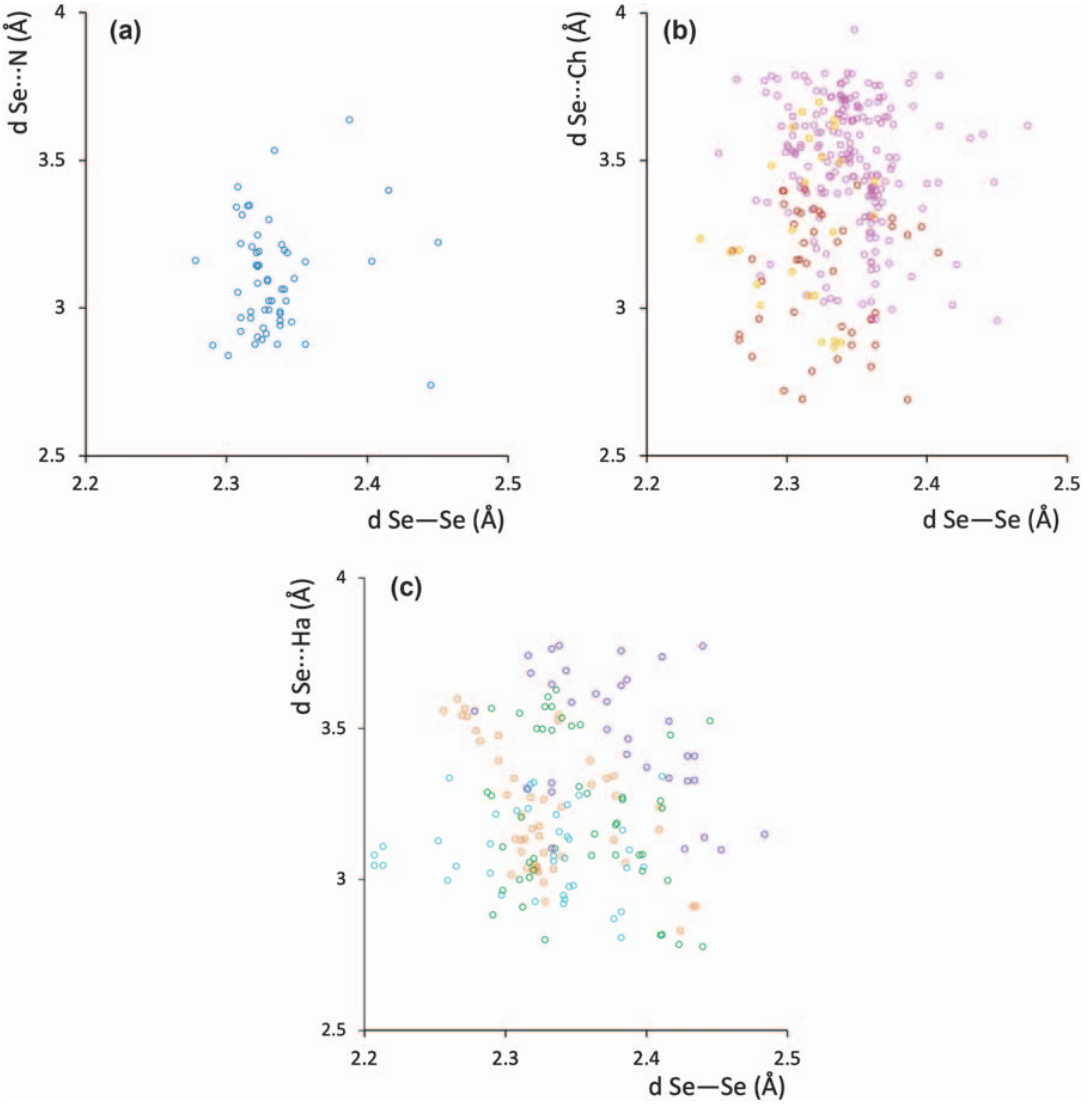

Figure 16.18 Scatterplots of $d_{Se\cdots Nu}$ *vs.* d_{Se-Se} distances in the Se–Se···Nu fragments for Nu = N (a); Ch (b); Ha (c). Nu colour codes: N = blue in (a); O = red, S = yellow, Se = magenta in (b); F = cyan, Cl = green, Br = orange, I = violet in (c).

Table 16.9 Occurrence, mean distances d [Å] (standard deviations s in parentheses), and δ values for Se–Se···Nu fragments.

Nu	Occurrence	d_{Se-Se} (s)	$d_{Se\cdots Nu}$ (s)	δ_{Se-Se} (%)	$\delta_{Se\cdots Nu}$ (%)
O	44	2.325 (0.04)	3.110 (0.22)	2.41	− 9.05
S	26	2.313 (0.03)	3.285 (0.27)	1.91	− 11.21
Se	209	2.350 (0.07)	3.487 (0.18)	3.53	− 8.21
N	54	2.336 (0.04)	3.086 (0.16)	2.93	− 10.56
Br	48	2.331 (0.04)	3.221 (0.21)	2.68	− 14.12
Cl	46	2.352 (0.045)	3.211 (0.26)	3.65	− 11.84
F	41	2.322 (0.05)	3.100 (0.14)	2.24	− 8.13
I	33	2.381 (0.05)	3.480 (0.22)	4.88	− 10.31

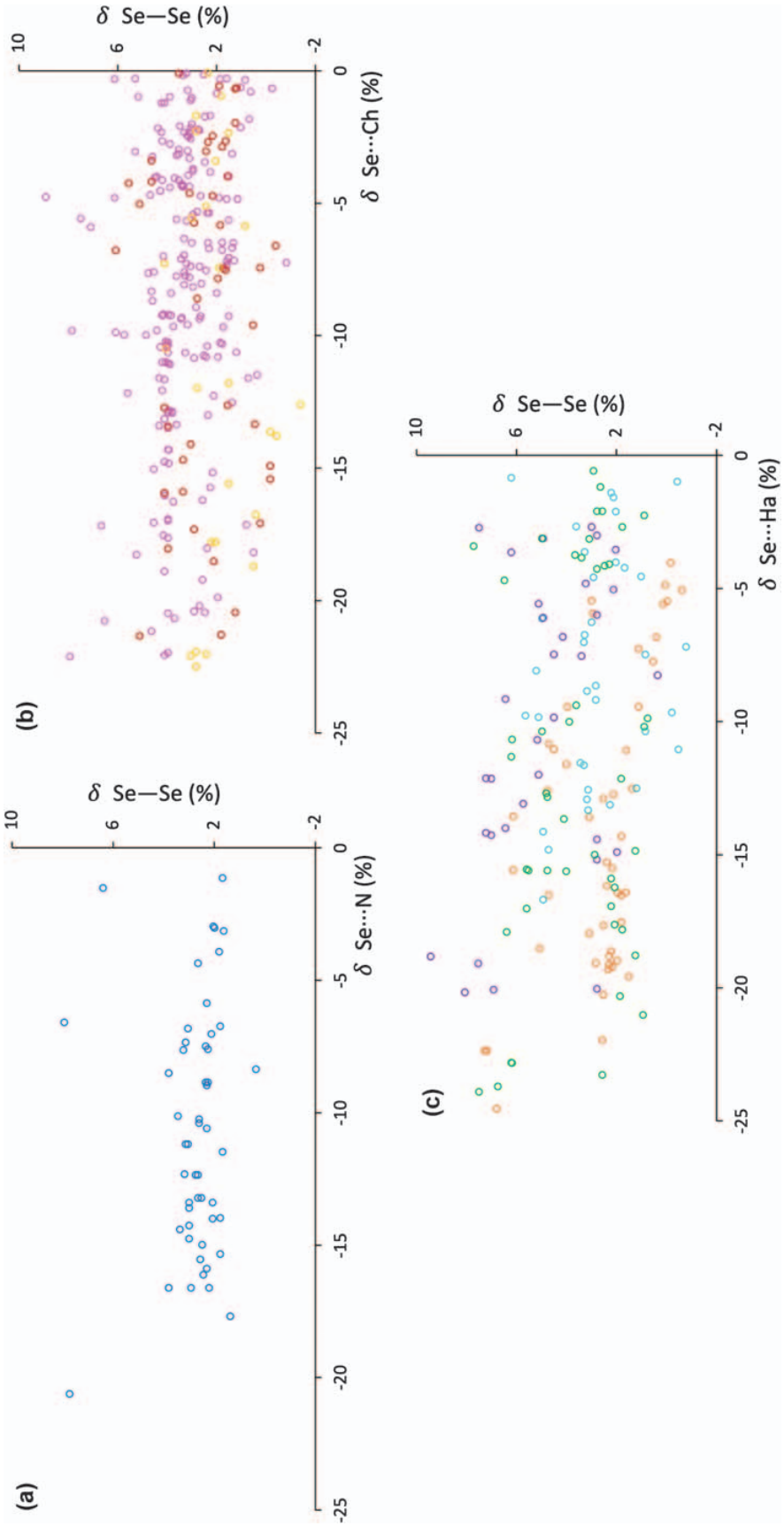

Figure 16.19 Scatterplots of δ_{Se-Se} *vs.* $\delta_{Se\cdots Nu}$ calculated for the Se–Se· · ·Nu fragments for Nu = N (a); Ch (b); Ha (c). Nu colour codes: N = blue in (a); O = red, S = yellow, Se = magenta in (b); F = cyan, Cl = green, Br = orange, I = violet in (c).

Interestingly, the values reported in Table 16.9 and Figure 16.19 indicate that the ChB interacting in Se–Se···Nu fragments are intermediate in strengths between those found in S–S···Nu and S–Se···Nu ones.

16.2.3 R–Te···Nu Fragments

The CSD lists 2318 linear fragments of the type R–Te···Nu (R = B, C, N, P, As, O, S, Se, Te and Nu = N, P, As, Sb, O, S, Se, Te, F, Cl, Br, I).[19] Following the choice adopted in the previous sections, the survey here reported is limited to categories of fragments with R = C, N, O, S, with the addition of Te to include compounds with Te–Te bonds, in analogy with S–S and Se–Se isologues. The histogram plot in Figure 16.20 shows the occurrence of fragments R–Te···Nu sorted by R and Nu, with an evident prevalence of C–Se···Nu systems (1769, 76.3%) followed by Te–Te···Nu (172, 7.4%), N–Te···Nu (120, 5.2%), O–Te···Nu (98, 4.2%), S–Te···Nu (68, 2.9%), and Ha–Te···Nu (34, 1.5%).

16.2.3.1 C–Te···Nu

The number of C–Te···Nu linear fragments amounts to 1769 with a prevalence for Nu = Ha and Ch (54.2% and 37.0%, respectively), the remaining 8.8% of occurrences being constituted by C–Te···N ones.[19] The compounds encompassed in this survey belong to various categories such as tellurophenes, tellurazoles, tellurafulvalente, telluroanhydrides, tellurocyanates, tellurides, and tellane derivatives.

The mean covalent and non-covalent bond distances calculated within the fragments C–Te···Nu show similar values [d_{C-Te} = 2.109 (0.03), 2.118 (0.03), and 2.127 (0.03) Å; $d_{Te\cdots Nu}$ = 3.16 (0.22), 3.43 (0.39), and 3.57 (0.22) Å, for

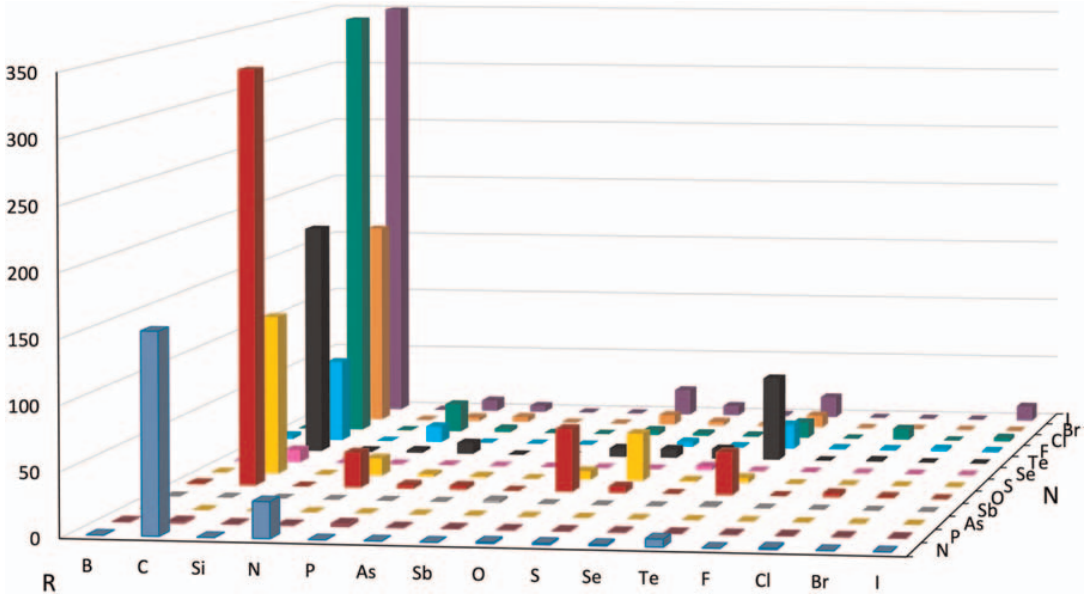

Figure 16.20 Linear R–Te···Nu fragment occurrence (R = B, C, Si, N, P, As, Sb, O, S, Se, Te, F, Cl, Br, I; Nu = N, P, As, Sb, O, S, Se, Te, F, Cl, Br, I) deposited at the CSD.

Nu = N, Ch, and Ha, respectively]. Despite the different vdW radii of the chalcogen atoms involved, non-bonding distances Se···Nu and Te···Nu fall in the same range and show very similar mean values. The scatterplots of Te···Nu *vs.* C–Te distances for Nu = N (a), Ch (b), and Ha (c) are reported in Figure 16.21 and display wide distributions of the values, particularly for the C–Se···Ha systems, as previously noticed for the selenium isologues (Figures 16.12c and 16.21c). Such wide distributions are in good agreement with the continuum from weak to strong Ch···Nu interactions noted for C–Te···I and C–Se···Br systems.[23]

The mean values calculated for the C–Te and Te···Nu distances in the fragments C–Te···Nu are summarized in Table 16.10, along with the mean of δ_{C-Te} and $\delta_{Te\cdots Nu}$ values calculated, as described above (eqn (16.1) and (16.2)). Figure 16.22 shows the scatterplots of δ_{C-Te} *vs.* $\delta_{Te\cdots Nu}$.

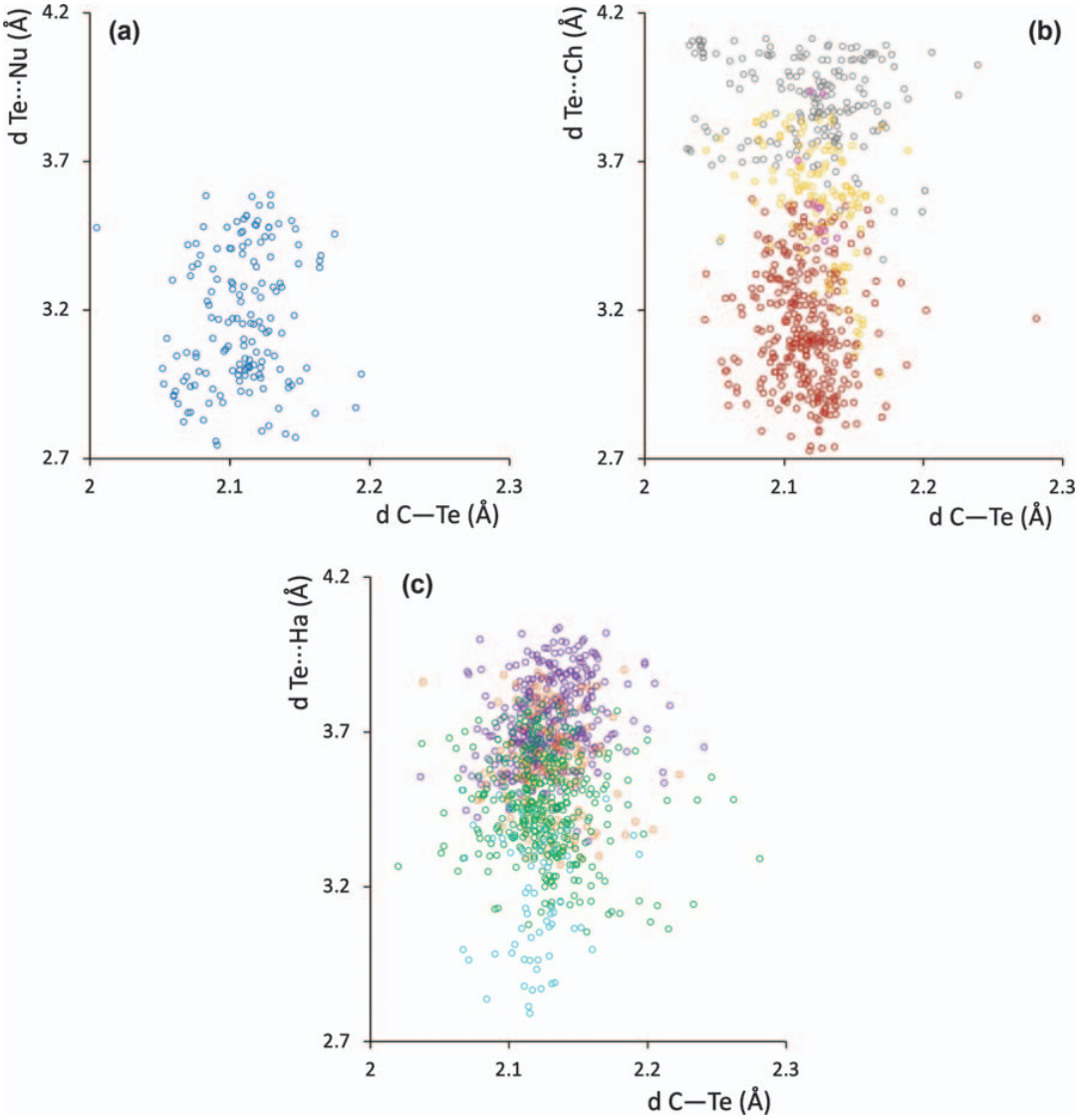

Figure 16.21 Scatterplots of $d_{Te\cdots Nu}$ *vs.* d_{C-Te} distances in the C–Te···Nu fragments for Nu = N (a); Ch (b); Ha (c). Nu colour codes: N = blue in (a); O = red, S = yellow, Se = magenta, Te = black in (b); F = cyan, Cl = green, Br = orange, I = violet in (c).

Table 16.10 Occurrence, mean distances d [Å] (standard deviation, s), and δ values for C–Te···Nu fragments.

Nu	Frequency	$d_{C–Te}$ (s)	$d_{Te···Nu}$ (s)	$\delta_{C–Te}$ (%)	$\delta_{Te···Nu}$ (%)
O	332	2.116 (0.03)	3.120 (0.17)	2.69	− 12.96
S	127	2.120 (0.04)	3.562 (0.20)	3.05	− 7.73
Se	10	2.125 (0.007)	3.602 (0.19)	3.15	− 9.03
Te	185	2.119 (0.04)	3.894 (0.15)	2.93	− 5.46
N	155	2.109 (0.03)	3.165 (0.22)	2.37	− 12.46
Br	165	2.129 (0.02)	3.588 (0.15)	3.33	− 8.25
Cl	352	2.126 (0.03)	3.460 (0.16)	3.09	− 9.39
F	66	2.119 (0.02)	3.153 (0.22)	2.78	− 10.89
I	376	2.128 (0.03)	3.729 (0.13)	3.30	− 7.69

The values of $\delta_{C–Te}$ vary in a range between 0% and 6% for almost all the fragments, without the loss of continuity found in the case of the isologues C–S···Nu and C–Se···Nu. The $\delta_{Se···Nu}$ values present values up to −13% indicating an increasing in strength of the ChBs involved on passing from C–Se···Nu to C–Te···Nu fragments.

16.2.3.2 N–Te···Nu

The number of linear fragments bearing a N–Te···Nu ChB amounts to 120 hits. These involve compounds usually corresponding to S- and Se-analogous, *i.e.*, tellurimide, amido-tellurium derivatives, and Te-containing heterocycles such as tellurazoles and a fused polycyclic derivative thereof. Among the linear N–Te···Nu fragments, the Nu atom is a nitrogen in 28 hits (23.3%), a chalcogen in 44 (36.7%), and a halogen species in 48 (40.0%). The mean distances N–Te and Te···Nu calculated for the three sub-categories display very close values [$d_{N–Te} = 2.052$ (0.05), 2.028 (0.07), and 2.009 (0.05) Å; $d_{Te···Nu} = 2.932$ (0.11), 3.19 (0.46), and 3.27 (0.28) Å for Nu = N, Ch, and Ha, respectively]. As noticed for the sulfur and selenium isologues, N–Te···Nu fragments show covalent and non-covalent distances notably shorter than those found in the analogous C–Te···Nu fragments, confirming the strengthening of the ChB donor ability on passing from carbon-bonded to nitrogen-bonded Te-donors, analogously to what previously described for ChB donors featuring S- and Se-atoms. The involved distances fall in a range common to all fragments, as well as the relative $\delta_{Te···Nu}$ and $\delta_{N–Te}$ values (Figure 16.23).

The mean N–Te and Te···Nu distances in fragments N–Te···Nu (Table 16.11) confirm the strengthening of the ChB on passing from selenium to tellurium with Te···Nu mean distances shorter than those found in the N–Se···Nu isologues, notwithstanding the larger Te vdW radium, and increased shortening $\delta_{Te···Nu}$ reaching mean values of about −19% for Nu = O and N (Table 16.11).

16.2.3.3 O–Te···Nu

Linear O–Te···Nu fragments involving a ChB amount to 98 hits with a net prevalence of systems featuring a chalcogen as the ChB acceptor (O–Te···O, 51%;

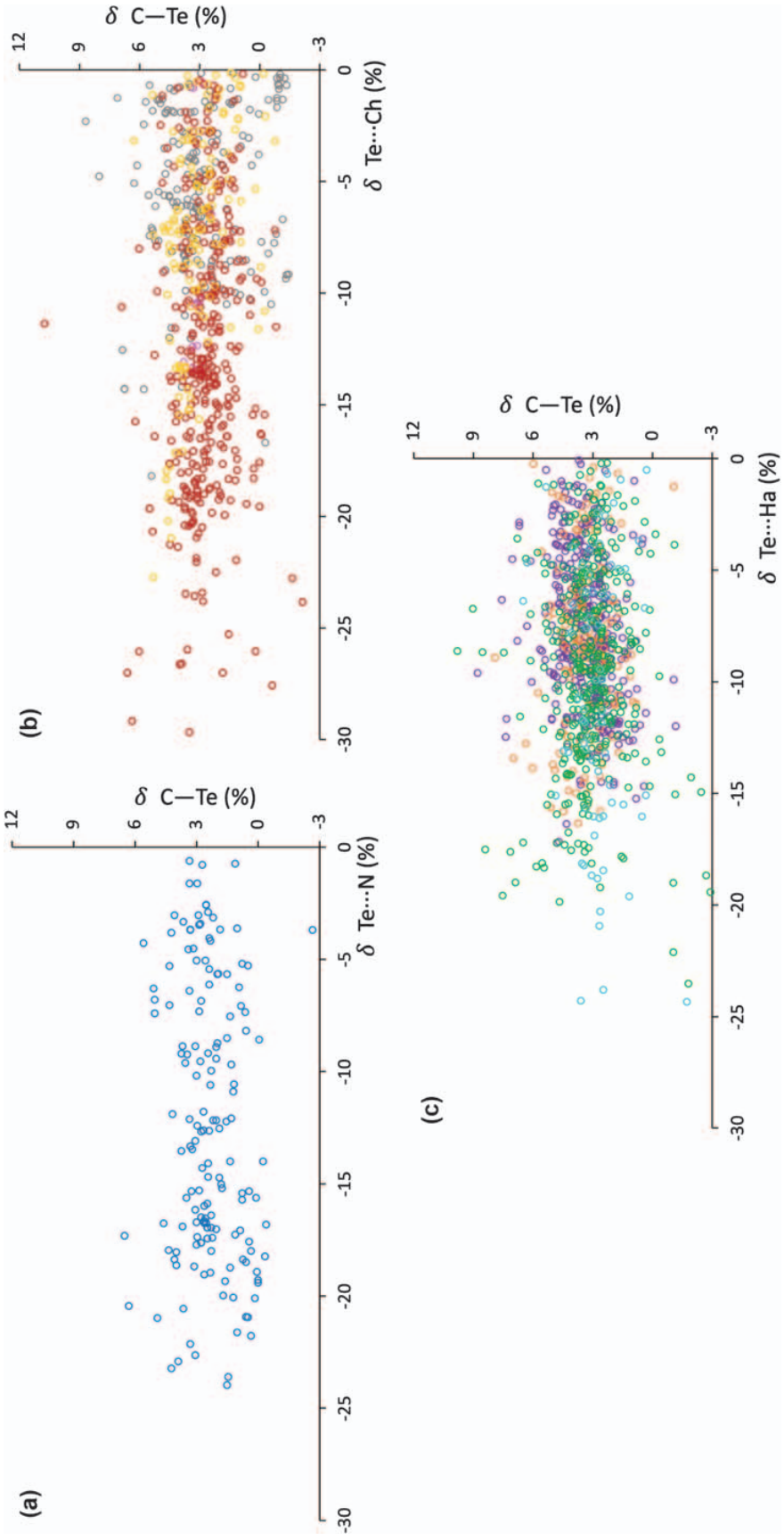

Figure 16.22 Scatterplots of δ_{C-Te} *vs.* $\delta_{Te\cdots Nu}$ calculated for the C–Te···Nu fragments for Nu = N (a); Ch (b); Ha (c). Nu colour codes: N = blue in (a); O = red, S = yellow, Se = magenta, Te = black in (b); F = cyan, Cl = green, Br = orange, I = violet in (c).

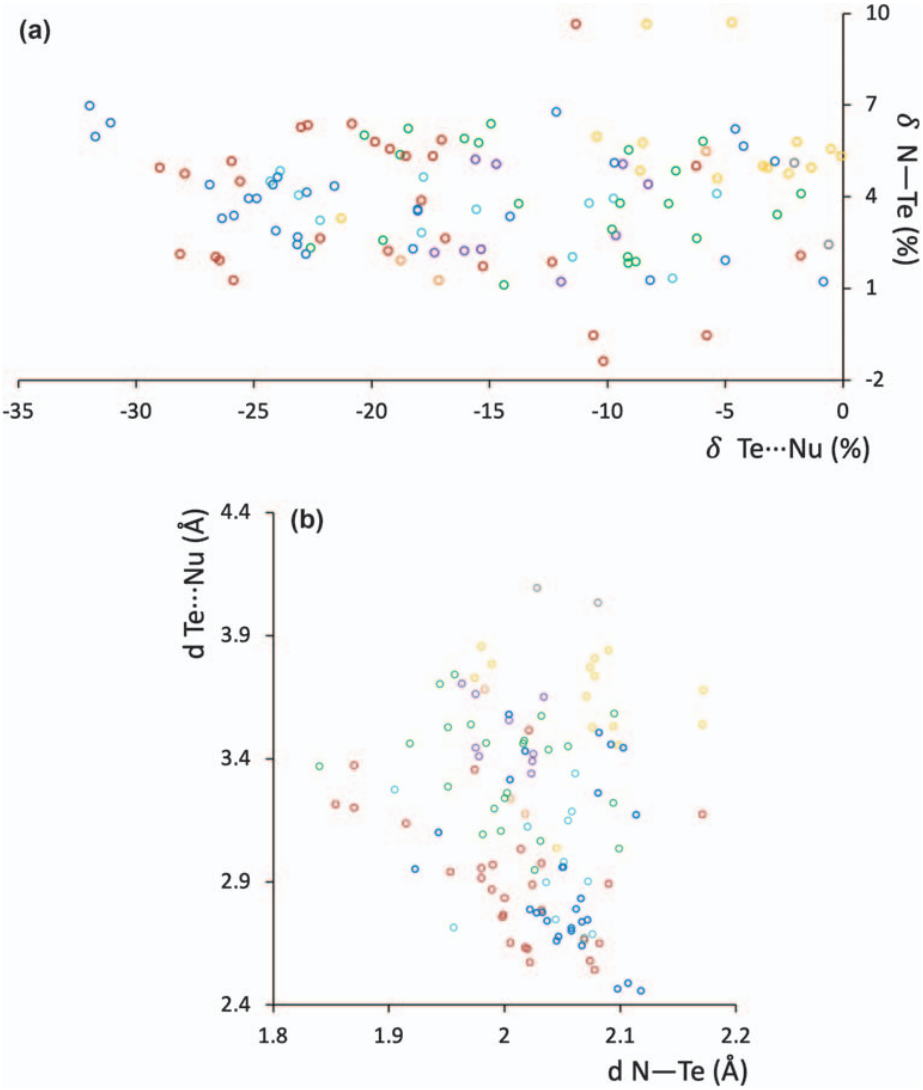

Figure 16.23 Scatterplots of δ_{N-Te} *vs.* $\delta_{Te\cdots Nu}$ (a) and $d_{Te\cdots Nu}$ *vs.* d_{N-Te} (b) for the N–Te···Nu fragments. Nu colour codes: N = blue, O = red, S = sulfur, Te = black, F = cyan, Cl = green, Br = orange, I = violet.

Table 16.11 Occurrence, mean distances *d* [Å] (standard deviation, s), and δ values for N–Te···Nu fragments.

Nu	Occurrence	d_{N-Te} (s)	$d_{Te\cdots Nu}$ (s)	δ_{N-Te} (%)	$\delta_{Te\cdots Nu}$ (%)
O	28	2.004 (0.07)	2.910 (0.26)	3.67	− 18.71
S	14	2.071 (0.06)	3.640 (0.21)	5.72	− 5.71
Te	2	2.054 (0.04)	4.065 (0.04)	3.76	− 1.33
N	28	2.052 (0.05)	2.932 (0.34)	4.00	− 18.77
Br	3	2.002 (0.02)	3.366 (0.28)	2.89	− 13.91
Cl	23	2.099 (0.06)	3.359 (0.22)	3.73	− 11.84
F	13	2.033 (0.05)	2.985 (0.23)	3.45	− 15.44
I	9	2.000 (0.03)	3.509 (0.14)	0.0337	− 13.13

O–Te···S, 7%, O–Te···Se, 7%, O–Te···I, 22%, O–Te···Cl, 8; O–Te···Br, 4%; O–Te···N, 1%).[19] The compounds comprised in this category mainly belong to the class of tellurium(IV) oxyanions, often showing complex polymeric structures.

Table 16.12 Occurrence, mean distances d [Å] (standard deviation, s), and δ values for O–Te···Nu fragments.

Nu	Occurrence	$d_{O–Te}$ (s)	$d_{Te\cdots Nu}$ (s)	$\delta_{O–Te}$ (%)	$\delta_{Te\cdots Nu}$ (%)
O	50	1.924 (0.07)	2.840 (0.33)	− 1.14	− 20.67
S	7	1.940 (0.04)	3.756 (0.03)	− 0.015	− 2.69
Te	7	2.090 (0.08)	3.835 (0.25)	2.46	− 6.91
Br	8	1.917 (0.004)	3.141 (0.03)	− 1.19	− 19.67
Cl	4	1.945 (0.04)	3.291 (0.25)	2.71	− 13.61
I	21	1.907 (0.017)	3.403 (0.13)	− 1.68	− 15.76

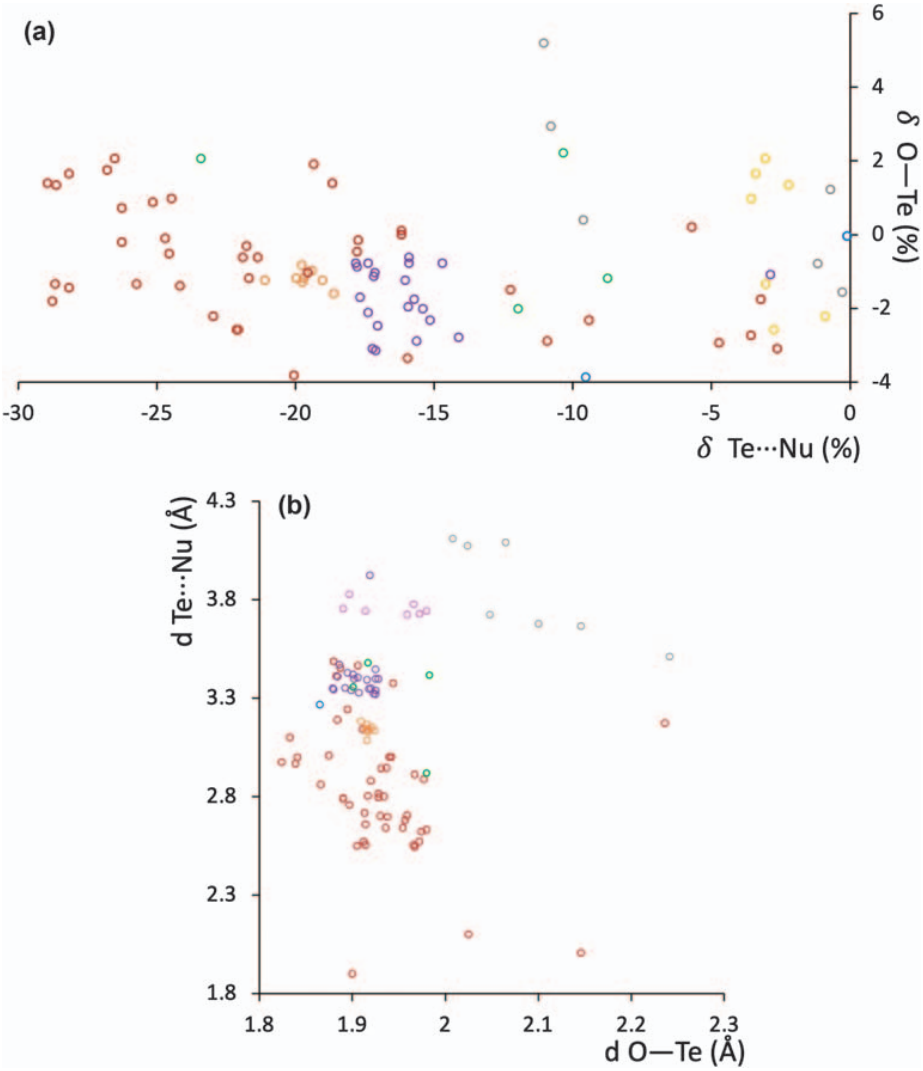

Figure 16.24 Scatterplots of $\delta_{O–Te}$ *vs.* $\delta_{Te\cdots Nu}$ (a) and $d_{Te\cdots Nu}$ *vs.* $d_{O–Te}$ (b) for the O–Te···Nu fragments. Nu colour codes: N = blue, O = red, S = sulfur, Te = black, Cl = green, Br = orange, I = violet.

The mean values calculated for the O–Te and Te···Nu distances in the fragments O–Te···Nu are summarized in Table 16.12, along with the delta $\delta_{O–Te}$ and $\delta_{Te\cdots Nu}$ mean values. Figure 16.24 shows the scatterplots of $\delta_{O–Te}$ *vs.* $\delta_{Te\cdots Nu}$ values (a) and Te···Nu *vs.* O–Te distances (b). The fragments display short covalent O–Te distances mainly falling in the range 1.8–2.0 Å

with only a few cases, mainly O–Te···Te ones, featuring distances longer than and 2.0 Å. The strength of the involved ChBs is increased with respect to the lighter sulfur and selenium isologues and to the analogous N–Te···Nu with the greater interactions regarding fragments involving O, Br, and Cl as the ChB acceptors.

16.2.3.4 S–Te···Nu

The 68 linear S–Te···Nu fragments found in the CSD are detailed in Table 16.13.[19] In these compounds Tellurium generally shows a metal character, being coordinated by the sulfur of thio- and dithiolates, thio- and dithiocarbamates, dithiophosphates and dithiophosphites, sulfonate, sulfides, and so on.

The S–Te···Nu fragments feature S–Te and Te···Nu values in the ranges 2.3–2.6, and 2.8–4.0 Å, respectively, and $\delta_{Te\cdots Nu}$ between −10% and −25%, with mean values slightly shorter than those recorded for the S–Se···Nu isologues (Table 16.13 and Figure 16.25).

16.2.3.5 Te–Te···Nu

A total number of 172 linear Te–Te···Nu fragments involving a ChB can be found in the CSD. The compounds in this category are mainly di- and polytellurides derivatives.[19] The fragments mainly involve a Te–Te···Te interaction (67 items, 39%). The occurrences of Te–Te···Nu fragments along with the mean Te–Te and Te···Nu distances and δ_{Te-Te} and $\delta_{Te\cdots Nu}$ values are listed in Table 16.14.

The values reported in Table 16.14, as well as the data reported in the Te–Te and Te···Nu distances and δ_{Te-Te} and $\delta_{Te\cdots Nu}$ scatterplots (Figure 16.26) show values well-suited with the presence of ChBs similar in strength to those found in the Se–Se···Nu fragments.

16.3 Conclusions

Notwithstanding the large number of scientific contributions on ChB interactions, a systematic survey of structural data was missing in the literature, being generally limited to selected groups of strictly related

Table 16.13 Occurrence, mean distances d [Å] (standard deviation, s), and δ values for S–Te···Nu fragments.

Nu	Occurrence	d_{S-Te} (s)	$d_{Te\cdots Nu}$ (s)	δ_{S-Te} (%)	$\delta_{Te\cdots Nu}$ (%)
O	5	2.367 (0.05)	2.983 (0.08)	−1.36	−16.66
S	38	2.411 (0.04)	3.389 (0.15)	0.475	−12.20
Te	7	2.419 (0.03)	3.697 (0.28)	7.80	−10.27
Br	3	2.442 (0.005)	3.196 (0.13)	1.76	−18.26
Cl	2	2.407 (0.03)	3.549 (0.07)	0.312	−6.86
F	4	2.312 (0.02)	3.059 (0.27)	−36.87	−13.34
I	8	2.509 (0.04)	3.247 (0.08)	4.526	−19.64

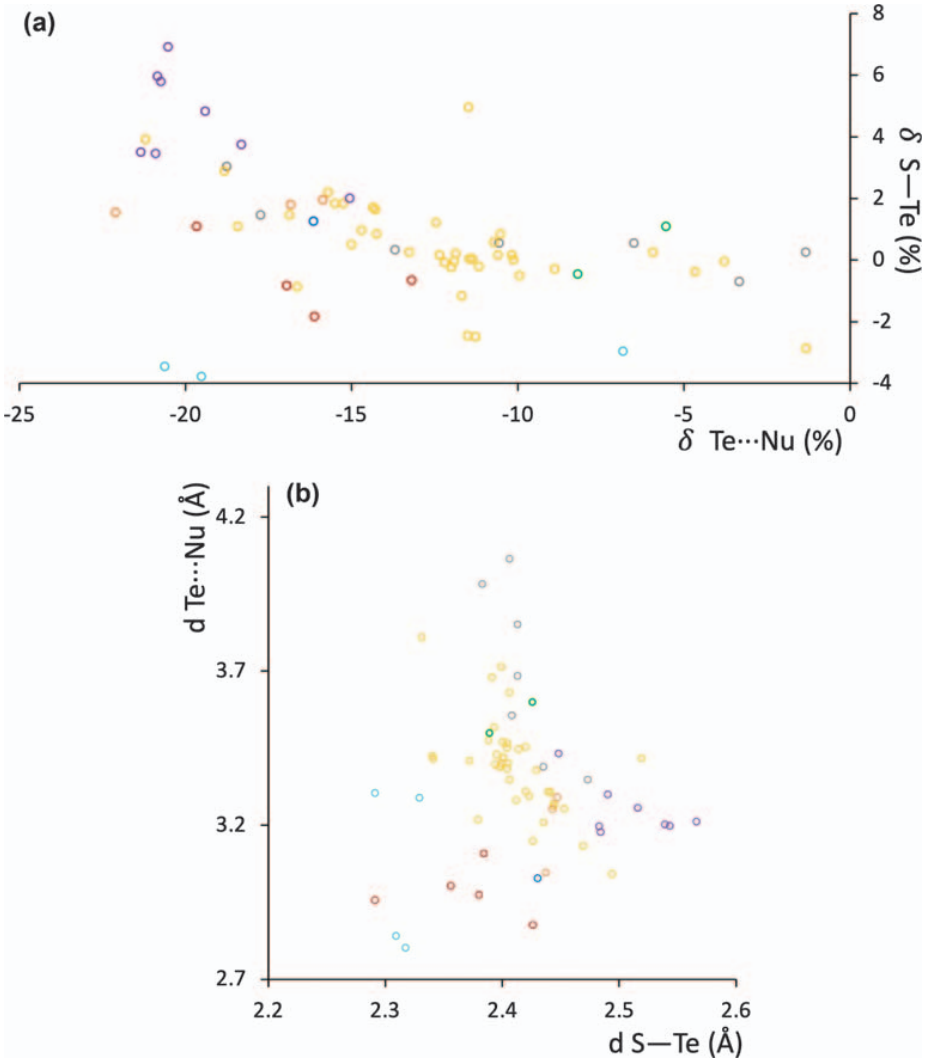

Figure 16.25 Scatterplots of δ_{S-Te} *vs.* $\delta_{Te\cdots Nu}$ (a) and $d_{Te\cdots Nu}$ *vs.* d_{S-Te} (b) for the S–Te···Nu fragments. Nu colour codes: N = blue, O = red, S = sulfur, Te = black, F = cyan, Cl = green, Br = orange, I violet.

Table 16.14 Occurrence, mean distances d [Å] (standard deviation, s), and δ values for Te–Te···Nu fragments.

Nu	Occurrence	d_{Te-Te} (s)	$d_{Te\cdots Nu}$ (s)	δ_{Te-Te} (%)	$\delta_{Te\cdots Nu}$ (%)
O	34	2.727 (0.06)	3.093 (0.21)	− 1.21	− 13.61
S	4	2.751 (0.04)	3.631 (0.03)	− 0.317	− 5.93
Te	67	2.774 (0.10)	3.753 (0.06)	0.510	− 8.92
N	6	2.697 (0.05)	3.300 (0.19)	− 2.29	− 8.58
Br	10	2.716 (0.06)	3.343 (0.23)	− 1.58	− 14.51
Cl	13	2.734 (0.06)	3.399 (0.25)	− 0.956	− 10.78
F	20	2.787 (0.16)	3.122 (0.23)	0.960	− 11.55
I	17	2.730 (0.06)	3.563 (0.22)	− 1.10	− 11.81

compounds. An analysis of all the structural data deposited at the CSD allows us to validate the assumptions generally accepted for ChB based on experimental or theoretical limited groups of compounds. The reported

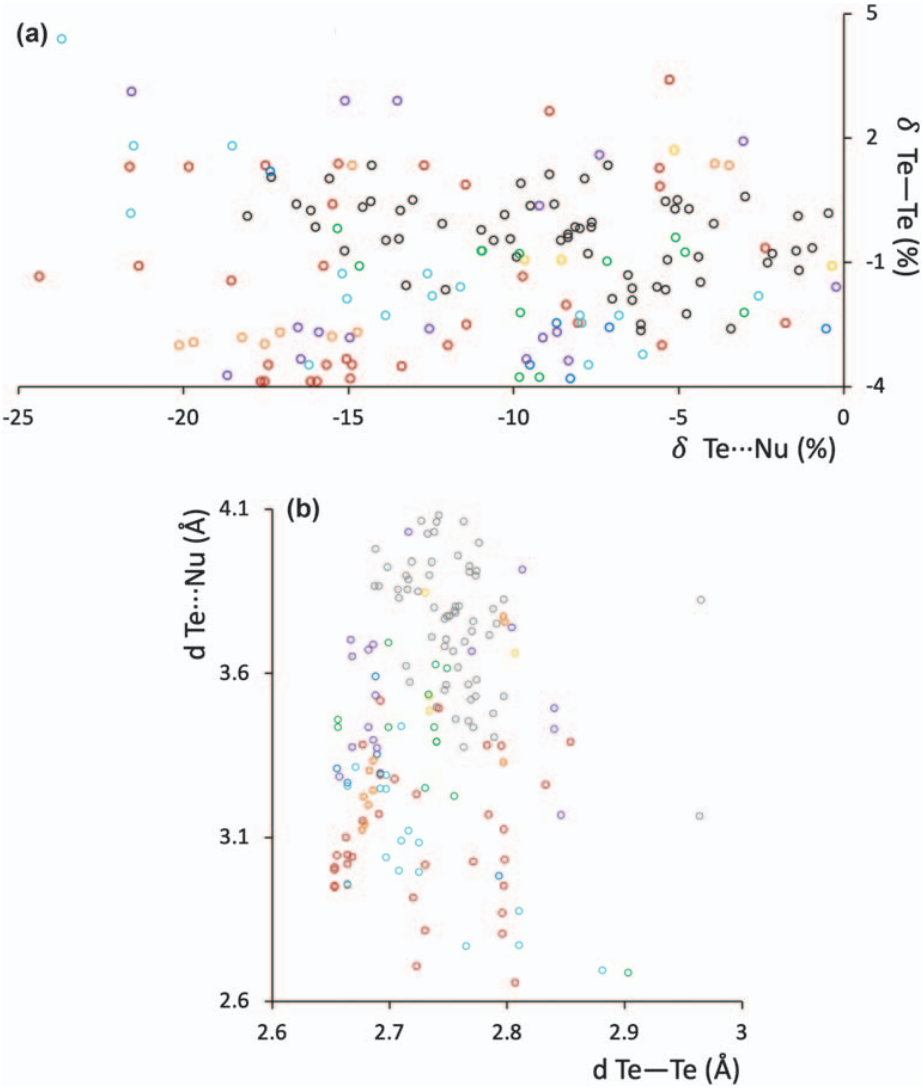

Figure 16.26 Scatterplots of $\delta_{\text{Te–Te}}$ *vs.* $\delta_{\text{Te}\cdots\text{Nu}}$ (a) and $d_{\text{Te}\cdots\text{Nu}}$ *vs.* $d_{\text{Te–Te}}$ (b) for the T–Te···Nu fragments. Nu colour codes: N = blue, O = red, S = sulfur, Te = black, F = cyan, Cl = green, Br = orange, I = violet.

structural data for the linear R–Ch···Nu fragments involving a ChB confirm a strengthening in the Ch···Nu interactions with the increasing of polarizability of the chalcogen atom (Te > Se > S). Notwithstanding the increase of the vdW radius of the relevant Ch atoms, the Ch···Nu non-bonding distances fall in a similar range 2.4–3.6, 2.4–3.8, and 2.4–4.1 Å for Ch = S, Se, and Te, respectively (Figure 16.27).

On the contrary, the region of existence of the fragments featuring a different R atom covalently bonded to the chalcogen atom can be clearly identified for the different R–Ch···Nu systems by the different values displayed by the R–Ch distances. The increase in strength of the involved ChBs is better evidenced by the function $\delta_{\text{Ch}\cdots\text{Nu}}$ (eqn (16.2)) that normalizes the difference between the Ch···Nu distances and the sum of the relevant vdW radii. Figure 16.28 reports the $\delta_{\text{Ch}\cdots\text{Nu}}$ *vs.* $\delta_{\text{R–Ch}}$ values calculated for the R–Ch···Nu fragments where Ch = S (a), Se (b), and Te (c).

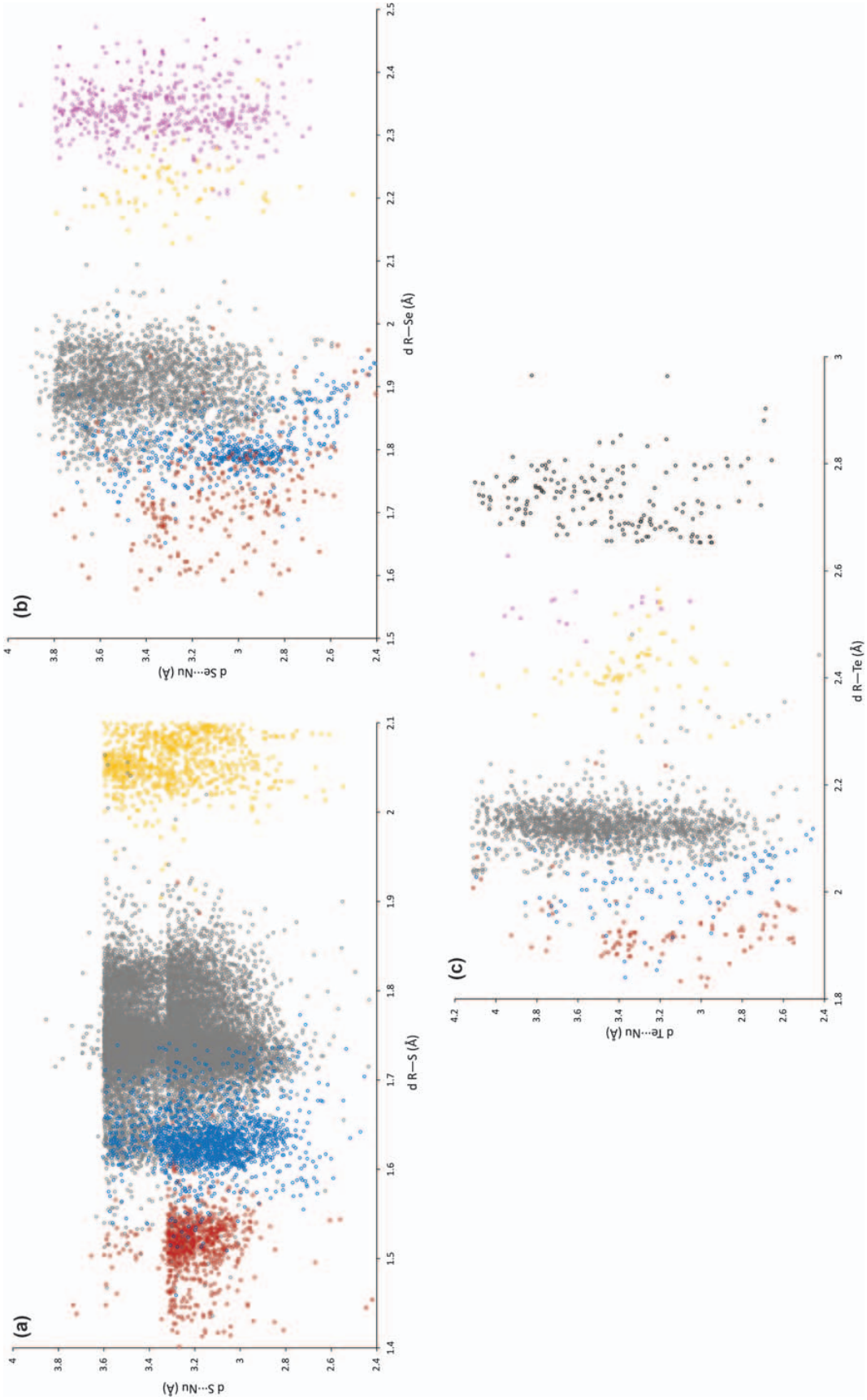

Figure 16.27 Scatterplots of $d_{S\cdots Nu}$ *vs.* $d_{R\text{–}S}$ (a); $d_{Se\cdots Nu}$ *vs.* $d_{R\text{–}Se}$ (b); $d_{Te\cdots Nu}$ *vs.* $d_{R\text{–}Te}$ (c) for the relevant R–Ch···Nu fragments. Nu colour codes: N = blue, O = red, S = sulfur, Se = magenta, Te = black, F = cyan, Cl = green, Br = orange, I = violet.

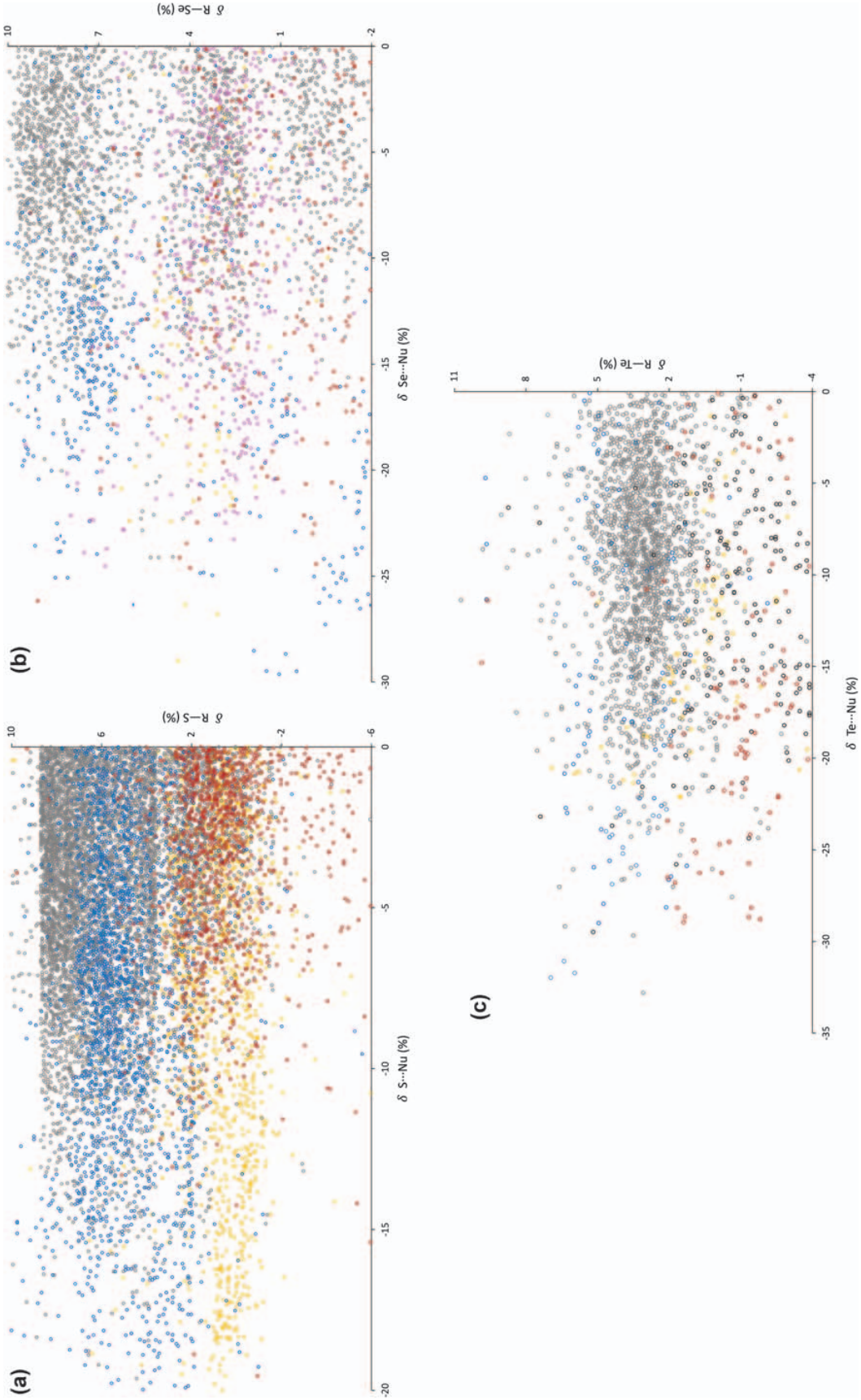

Figure 16.28 Scatterplots of the $\delta_{\text{R-Ch}}$ *vs.* $\delta_{\text{Ch}\cdots\text{Nu}}$ values calculated for the R–Ch···Nu fragments for Ch = S (a); Se (b); Te (c). Nu colour codes: N = blue, O = red, S = sulfur, Se = magenta, Te = black, F = cyan, Cl = green, Br = orange, I = violet.

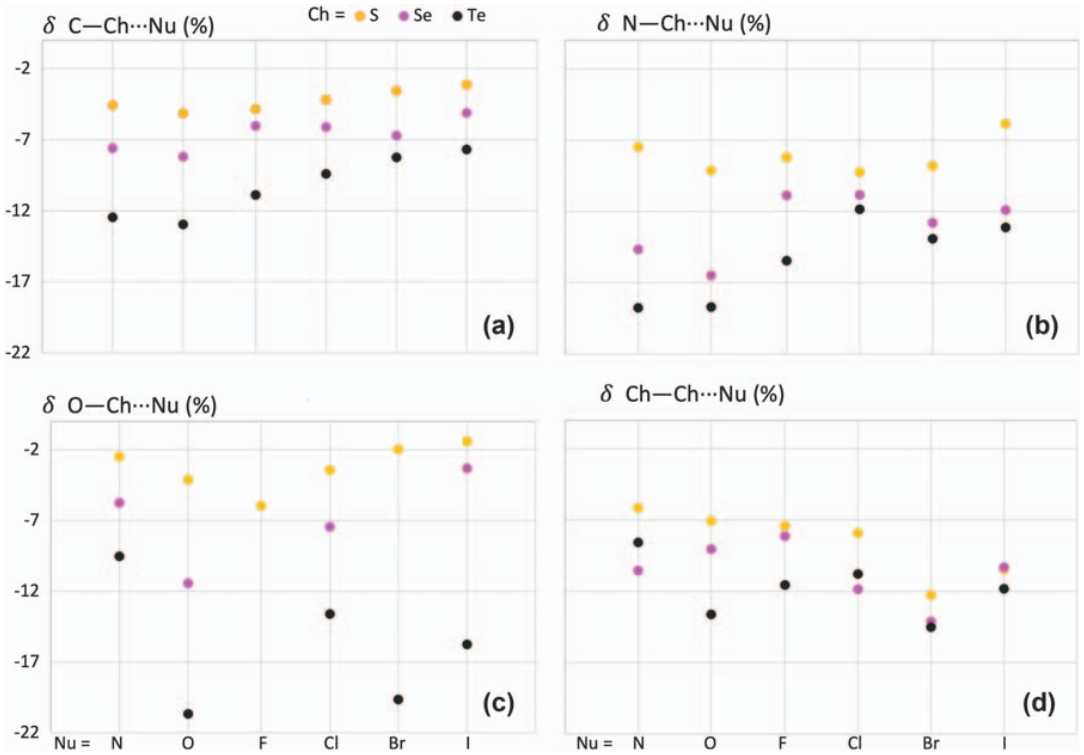

Figure 16.29 Mean $\delta_{Ch\cdots Nu}$ values calculated for the R–Ch···Nu fragments [R = C (a); N (b); O (c); Ch (S–S, Se–Se, and Te–Te) (d)]. Nu = N, O, F, Cl, Br, I. Ch colour codes: S = yellow, Se = magenta, Te = black.

The scatterplots of the δ_{R-Ch} *vs.* $\delta_{Ch\cdots Nu}$ values for the fragments R–Ch···Nu show similar variation ranges in the covalent distances R–Ch and an increasing in difference with respect to the sum of the involved vdW radii in the order Te > Se > S confirming a corresponding increasing of the pertinent ChB interactions. The increase in the ChB strength on passing from S to Se and Te is well represented by the mean values calculated for the function $\delta_{Ch\cdots Nu}$ for the different fragments with Nu = N, O, Ch (*i.e.*, S for S, Se for Se, and Te for Te), and Ha, reported in detail in Tables 16.1–16.14, and showed in Figure 16.29.

Less regular is the effect recorded for the fragments R–Ch···Nu on varying the nature of the R atom directly bonded to the Ch ones (Figure 16.30). The strength of the ChB increases when enhancing the electron-withdrawing character of the substituents, and a clear trend is observed on passing from C–Ch···Nu to N–Ch···Nu fragments for the all the examined systems and for all the involved Ch atoms (see Tables 16.1–16.14 and Figure 16.30). Fragments S–Ch···Nu also involve ChBs stronger than those found in C–Ch···Nu systems. On the contrary, a comparison between S–Ch···Nu and N–Ch···Nu fragments shows that the strength of the relative ChB interactions, usually higher when the chalcogen is covalently bonded to a nitrogen, can show increased values for the S–Ch···Ha systems, where the ChB acceptor Nu is a halogen species. With few exceptions, O–Ch···Nu fragments show the weakest ChB interactions, probably due to the nature of the involved compounds that are mainly chalcogen-oxides. The ChB formed by Se–Se···Nu

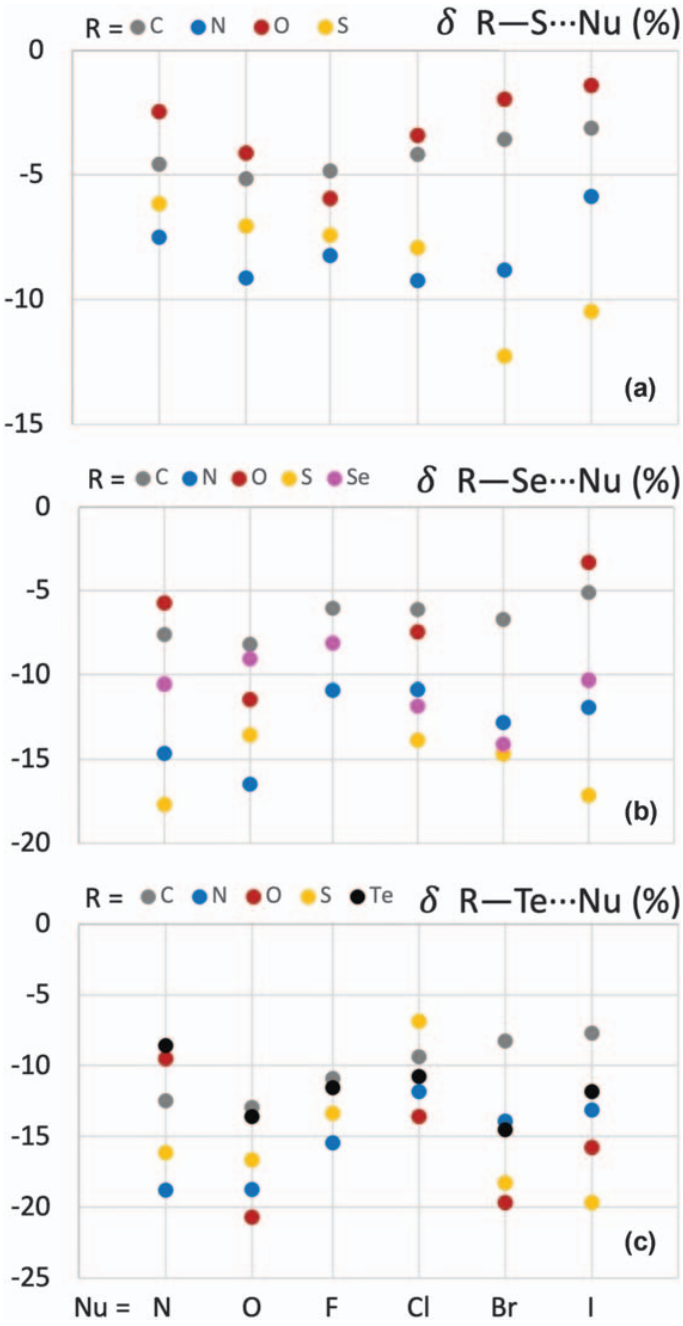

Figure 16.30 Mean δ_{Ch-Nu} values calculated for the R–Ch···Nu fragments [Ch = S (a); Se (b); Te (c)]. Nu = N, O, F, Cl, Br, I. R colour codes: C = grey, N = blue, O = red, S = yellow, Se = magenta, Te = black.

and Te–Te···Nu fragments display a strength very similar to those found in analogous C–Se···Nu and C–Te···Nu systems.

References

1. P. Scilabra, G. Terraneo and G. Resnati, *Acc. Chem. Res.*, 2019, **52**, 1313.
2. R. E. Rosenfield, R. Parthasarathy and J. D. Dunitz, *J. Am. Chem. Soc.*, 1977, **99**, 4860.

3. J. S. Murray, P. Lane, T. Clark and P. Politzer, *J. Mol. Model.*, 2007, **13**, 1033.
4. C. B. Aakeroy, D. L. Bryce, G. R. Desiraju, A. Frontera, A. C. Legon, F. Nicotra, K. Rissanen, S. Scheiner, G. Terraneo, P. Metrangolo and G. Resnati, *Pure Appl. Chem.*, 2019, **91**(11), 1889.
5. (a) The covalent radii utilized in the present work were taken from the work of B. Cordero, V. Gomez, A. E. Platero-Prats, M. Revés, J. Echeverrìa, E. Cremades, F. Barragàn and S. Alvarez, *Dalton Trans.*, 2008, 2832; (b) for atoms involved in single bonds, and from the work of P. Pyykkç and M. Atsumi, *Chem. – Eur. J.*, 2009, **15**, 12770, for atoms involved in multiple bonds.
6. K. T. Mahmudov, M. N. Kopylovich, M. F. C. Guedes da Silva and A. J. L. Pombeiro, *Dalton Trans.*, 2017, **46**, 10121.
7. L. Vogel, P. Wonner and S. M. Huber, *Angew. Chem., Int. Ed.*, 2019, **58**, 1880.
8. N. Biot and D. Bonifazi, *Coord. Chem. Rev.*, 2020, **413**, 213243.
9. M. Fourmigué and A. Dhaka, *Coord. Chem. Rev.*, 2020, **403**, 213084.
10. P. Politzer, J. S. Murray and T. Clark, *Phys. Chem. Chem. Phys.*, 2010, **12**, 7748.
11. V. Oliveira, D. Cremer and E. Kraka, *J. Phys. Chem. A*, 2017, **121**, 6845.
12. J. S. Murray, P. Lane, T. Clark and P. Politzer, *J. Mol. Model.*, 2007, **13**(10), 1033.
13. R. Bader, *Atoms in Molecules: A Quantum Theory*, Oxford University Press, USA, 1994, ISBN 978-0-19-855865-1.
14. M. C. Aragoni, M. Arca, F. A. Devillanova, F. Isaia and V. Lippolis, *Cryst. Growth Des.*, 2012, **12**, 2769.
15. N. Tarannam, R. Shukla and S. Kozuch, *Phys. Chem. Chem. Phys.*, 2021, **23**, 19948.
16. J. Zhang, W. Li, J. Cheng, Z. Liua and Q. Li, *RSC Adv.*, 2018, **8**, 26580.
17. D. Esrafili and R. Nurazar, *Mol. Phys.*, 2016, **114**, 276.
18. L. M. Azofra, I. Alkorta and S. Scheiner, *J. Phys. Chem. A*, 2015, **119**, 535.
19. CDS searches were made by ConQuest Version 2021.3.0 on Q_A–Ch$\cdots$$Q_B$ fragments by imposing a Q_A–Ch$\cdots$$Q_B$ angle between 160 and 180°. Ch$\cdots$$Q_B$ distances were imposed to be shorter than the sum of relevant van der Waals radii. Q_A = B, C, N, P, As, Sb, O, S, Se, Te, F, Cl, Br, I; Q_B = N, P, As, Sb, O, S, Se, Te, F, Cl, Br, I; Ch = S, Se, Te.
20. A. S. Lundemba, D. D. Bibelayi, P. A. Wood, J. Pradon and Z. G. Yava, *Acta Crystallogr.*, 2020, **B76**, 707.
21. A. J. Peloquin, C. D. McMillen, S. T. Iacono and W. T. Pennington, *ChemPlusChem*, 2021, **86**, 549.
22. P. Sanz Camacho, K. S. Athukorala Arachchige, A. M. Z. Slawin, T. F. G. Green, J. R. Yates, D. M. Dawson, J. D. Woollins and S. E. Ashbrook, *J. Am. Chem. Soc.*, 2015, **137**, 6172.
23. D. K. Miller, I. Y. Chernyshov, Y. Torubaev and S. Rosokha, *Phys. Chem. Chem. Phys.*, 2022, DOI: 10.1039/d1cp05441d.

AQ:4